Supplementary Information for

A phenyl-removal strategy for accessing an efficient dual-state emitter in the red/NIR region guided by TDDFT calculations

*Guomin Xia[a], Qingqing Shao[b], Kangli Liang[b], Yigang Wang[b], Lixia Jiang[a], Hongming Wang[a, b, *]*

[a] Institute for Advanced Study and College of Chemistry, Nanchang University, 999 Xuefu Road, Nanchang, 330031, P.R. China

[b] School of Materials Science and Technology, Nanchang University, 999 Xuefu Road, Nanchang, 330031, P.R. China

[*]Corresponding author: Hongming Wang; E-mail: hongmingwang@ncu.edu.cn

Table of Content

1. Computational methods and results

1.1 Computational methods

All calculations were performed using Gaussian 09 package[1]. Theoretical calculations for the geometrical optimizations was performed by density functional theory (DFT) and time-dependent DFT (TD-DFT) using B3LYP method.[2, 3] The 6-311G+(d, p) basis sets were employed for C, H, O and N atoms. We ascertained that all the transition states have only one imaginary frequency through vibrational analysis. The vibrational frequency was calculated at the same level to characterize the nature of the stationary points as true minima (with no imaginary frequency) or transition states (with unique imaginary frequency). In order to compare with the experiment, toluene was selected as the solvent for all the calculations using the integral equation formalism variant of the polarizable continuum model (IEFPCM). The zero-point vibrational energy (ZPE) and thermal corrections was also obtained by frequency calculations.

1.2 Computational results

The optimized geometries and calculated photoreaction potential energy profiles of **SQTPE** in ground (S0) and exited (S1) states were presented in Figure S1, in which there existed two competitive reaction channels both in S0 and S1 states. In S1 state, one occurred directly between S1R and S1P1 through TS2 accompanying the distortion of C1-N1 bond with an energy barrier of 3.27 kcal mol^{-1} and an exothermic process of 3.16 kcal mol^{-1}. From HOMO and LUMO orbitals of S1P1 in Figure S2, the densities of HOMO were mainly localized in phenylamine, while most densities were transferred to indole group in the LUMO. This result indicated that the process of C1-N1 bond distortion in S1 state involved more obvious TICT character, associated with dihedral angle ∠O1C1N1H1 changed from 0° of S1R to 93.73° of S1P1. The equilibration between a relaxed perpendicular conformer (S1P1) and a coplanar conformer (S1R) resulted in dual fluorescence band, through relaxation (534 nm) from the locally excited (LE) state and through red-shifted emission (576 nm) from TICT state to return to the ground state, respectively. The other channel in S1 state was that the ESIPT from N1 to O1 atom occurred between S1R and S1P2 via TS3 with an energy barrier of 12.30 kcal mol^{-1} and a heat release of 11.92 kcal mol^{-1}, rather than from N1 to the O atom of ether group with an increased total energies both in S0 and S1 states (see Figure S3a). In S1 state, the hydrogen bond between H1 and O1 was shorted from

2.896 Å in S1R to 1.237 Å in TS3 then 0.979 Å in S1P2, respectively (Table S1). Following proton transfer, the ESIPT state returned to the ground state through more red-shifted emission (638 nm). Because of lower energy barrier, the TICT channel was easier to occur than the ESIPT channel in solution. While TICT was greatly prohibited because of the strong interaction between molecules in crystalline state, thereby ESIPT process was favored. As for S0 state, due to strong endothermic, both proton transfer and C1-N1 bond distortion processes were difficult to occur. Similar photophysical processes were also observed in **SQHTPE**, **SQDP** and **SQP** (Figure S1-2 and Table S1), suggesting their very analogical ground/exited-state electronic structures in solution. Meanwhile, the red-shifted absorption peaks also revealed that the effective π conjugations was in the order of **SQHTPE** (530 nm) ≈ **SQDP** (528 nm) > **SQTPE** (514 nm) ≈ **SQP** (511 nm).

It was easy to conclude that the dual emission of all these molecules can be responded by their LE/TICT process in S1 state occurred in solution, while the red-shifted single emission was due to the favorable ESIPT process from N1 to O1 atoms in crystalline state. From the DFT calculations, the energy barrier of TS2 and reversion energy barrier of RTS2 was both enhanced with remove of one phenyl rotator from **SQTPE** to **SQHTPE**, which would cause less TICT formation and quickly thermodynamic equilibrium that consumed less the exciton energies in solution, thus led to more efficient Φ_{PL} of **SQHTPE** than that of **SQTPE** even if taking no account of the internal phenyl rotations in TPE segment. As for **SQDP** with two phenyl rotators removed, the thing became complex because **SQDP** hold more TICT formation with a relatively small value of TS2 from calculations, it seems that it should exhibit a low Φ_{PL} in solution as compared to that of **SQTPE**, but its Φ_{PL} in practical would become unforeseeable when we took account of the decreasing internal phenyl rotations in **SQDP**. With remove of three phenyl rotators, the obtained **SQP** hold a much lower value of TS2 of 1.38, which means that much more TICT formation and slow thermodynamic equilibrium that consuming great excited energy thereby led to much lower Φ_{PL} in solution, from a calculational viewpoint. As such, it is of great necessity to verify all the results through experiment data, which would help us to comprehensively evaluate all the impact factors in this system.

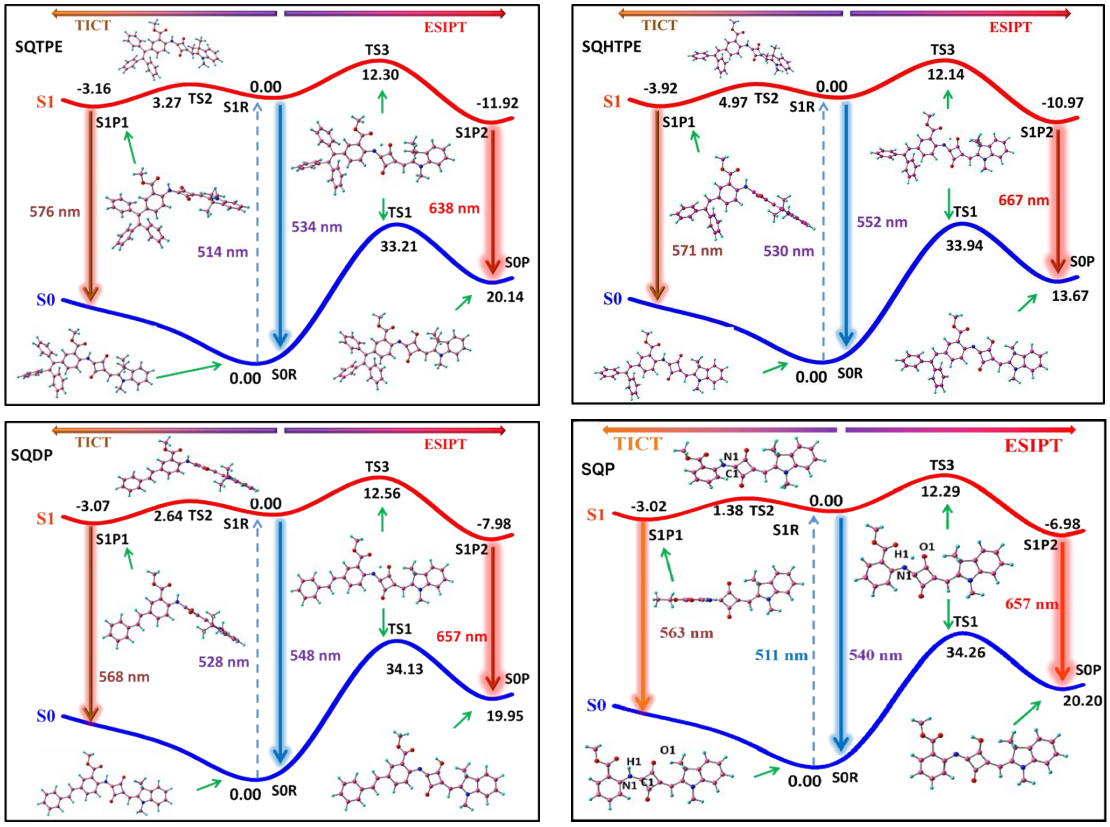

Figure S1. Calculated potential energy profiles (kcal mol^{-1}) and wavelengths (nm) of vertical excitation and emission of **SQTPE**, **SQHTPE**, **SQDP** and **SQP**.

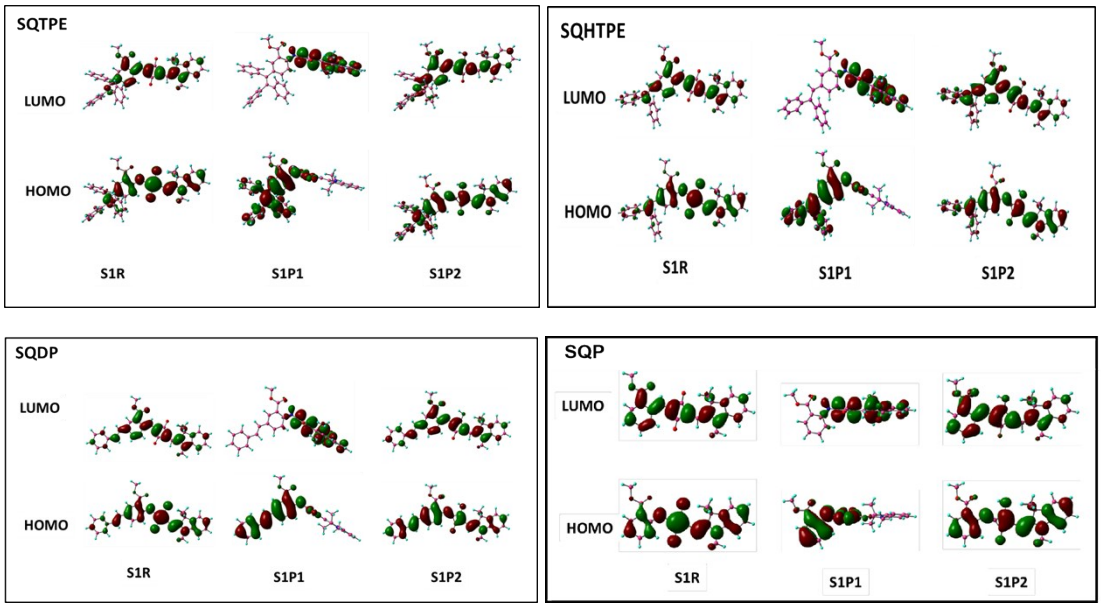

Figure S2. The HOMO and LUMO images of S1R, S1P1 and S1P2 in the photochemical reaction of **SQTPE**, **SQHTPE**, **SQDP** and **SQP**.

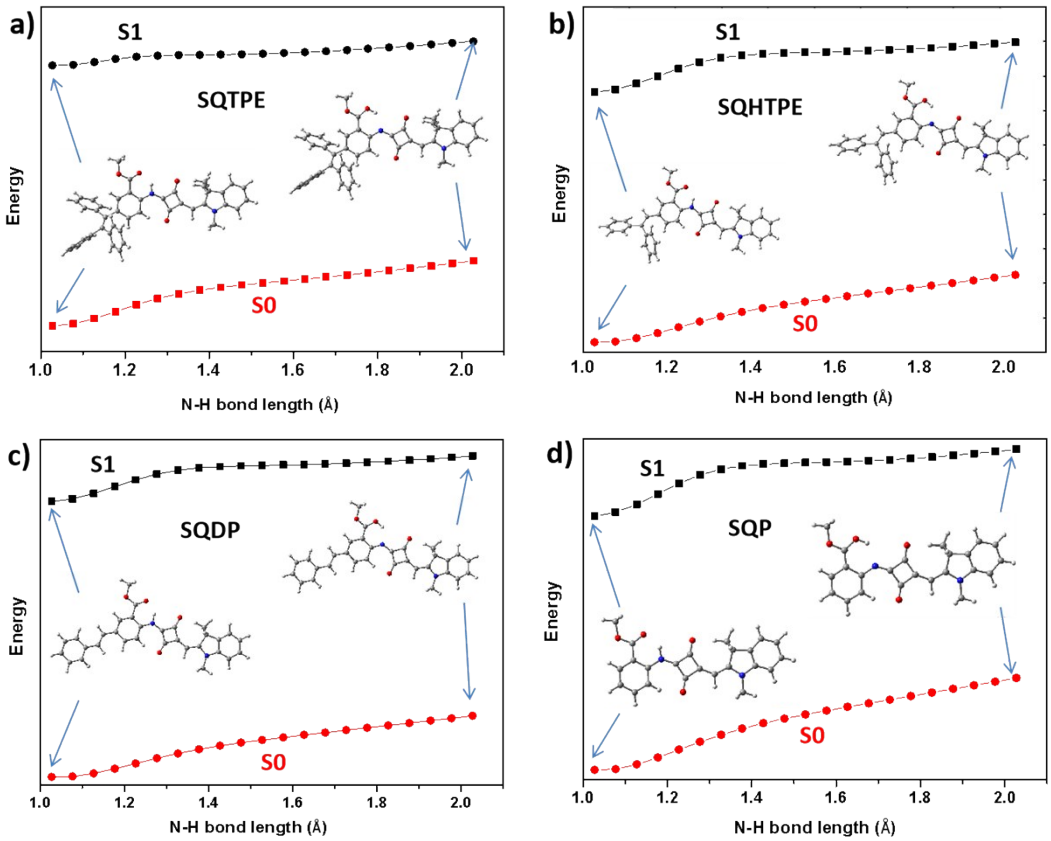

Figure S3. The scan of PES of S1 state of a) **SQTPE**, b) **SQHTPE**, c) **SQDP** and d) **SQP** as a function of N-H bond length.

Table S1. The hydrogen bond length (Å) and dihedral angles in **SQTPE**, **SQHTPE**, **SQDP** and **SQP** in S1 and S0 states.

Luminogen	Structure	N1-H1	H1-O1	∠O1C1N1H1
SQTPE	S0R	1.027	2.852	0
	S1R	1.027	2.896	0
	TS3	1.421	1.237	
	S1P2	2.507	0.979	
	S0P	2.547	0.978	
	TS1	1.388	1.255	
	TS2			50.24
	S1P1			93.73
SQHTPE	S0R	1.025	2.838	0
	S1R	1.028	2.873	0
	TS3	1.826	1.460	
	S1P2	2.529	0.974	
	S0P	0.974	2.58	
	TS1	1.388	1.259	
	TS2			51.42
	S1P1			90.56
SQDP	S0R	1.025	2.843	0
	S1R	1.029	2.872	0
	TS3	1.370	1.260	
	S1P2	2.518	0.976	
	S0P	2.568	0.974	
	TS1	1.388	1.254	
	TS2			58.00
	S1P1			91.74
SQP	S0R	1.025	2.842	0
	S1R	1.031	2.880	0
	TS3	1.418	1.241	
	S1P2	2.551	0.968	
	S0P	2.567	0.974	
	TS1	1.389	1.258	
	TS2			36.54
	S1P1			91.28

2 Materials and instruments

All chemicals and solvents were purchased from commercial suppliers and used as received unless explicitly stated. ^{1}H NMR and ^{13}C NMR spectra were measured on a Bruker AVANCE 400 spectrometer in $CDCl_3$ using TMS as an internal standard. UV-visible absorption spectra were recorded on a Lambda 750 spectrophotometer. Photoluminescence (PL) spectra were recorded on a Horiba FluoroMax-4 luminescence spectrometer. The absolute PL quantum efficiencies (Φ_{PL}) were determined using a Horiba FL-3018 Integrating Sphere. The fluorescence lifetime measurement was performed on a Horiba FluoreCube spectrofluorometer system using a UV diode laser (NanoLED 456 nm) for excitation. SEM images were collected on a Hitachi S-4300 instrument. Mass spectra were obtained with Trip TOFTM 5600 mass spectrometers. Thermogravimetric analysis (TGA) was carried out on a Dimand TG/DTA instrument at a heating rate of 5 ℃ min^{-1} under N_2 atmosphere. Powder X-ray diffraction (PXRD) data were collected using a XD-2 Purkinje multi crystal X-ray diffractometer in parallel beam geometry employing CuKα radiation at 40 kV and 30 mA. The diffraction data were collected in the 2θ range from 4 to 30° at the scanning speed of 1.54 second per step with 2θ step increment of 0.02°. The X-ray diffraction experiments were carried out on a Bruker SMART APEX-II Single-crystal diffractometer at room temperature. All the structures were resolved and analyzed with the assistance of shelxl-97 software. Semisquaraine was prepared according to the literature procedure.[4]

3 Syntheses

3.1 Synthesis of SQP

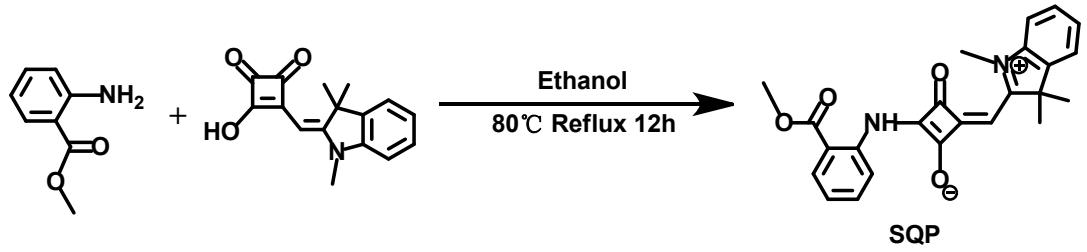

Scheme S1. The overall route for synthesis of **SQP**.

To a 50 mL round bottom flask was added semisquaraine (538 mg, 2 mmol) and methyl anthranilate (302 mg, 2 mmol) in 20 mL distilled EtOH. After reflux for 12 h at 80 ℃, the mixture was cooled to room temperature, the organic solvent was removed in vacuo. The crude product was then purified via column chromatography (CH_2Cl_2: CH_3OH = 100 : 1) to yield red product **SQP** (498 mg, 1.24mmol, 62%). ^{1}H NMR (400 MHz, $CDCl_3$, δ): 11.67 (s, 1H), 8.76 (d, J = 8.45 Hz, 1H), 8.00 (d, J = 7.90 Hz, 1H), 7.62 (t, J = 7.69 Hz, 1H), 7.33 (m, J = 15.29, 7.58 Hz, 2H), 7.17 (t, J = 7.38 Hz, 1H), 7.11 (t, J = 7.56 Hz, 1H), 7.04 (d, J = 7.94 Hz, 1H), 5.97 (s, 1H), 3.94 (s, 3H), 3.59 (s, 3H), 1.74 (s, 6H). ^{13}C NMR (100 MHz, $CDCl_3$, δ): 172.90, 168.13, 139.95, 135.03, 131.05, 127.94, 124.42, 123.64, 122.28, 121.36, 121,33, 115.45, 109.63, 52.61, 49.57, 26.99. HRMS m/z: [**SQP**+**H**]$^+$ calcd. for $C_{24}H_{22}N_2O_4$, 403.1652; found, 403.1659.

3.2 Synthesis of SQDP

Synthesis of a

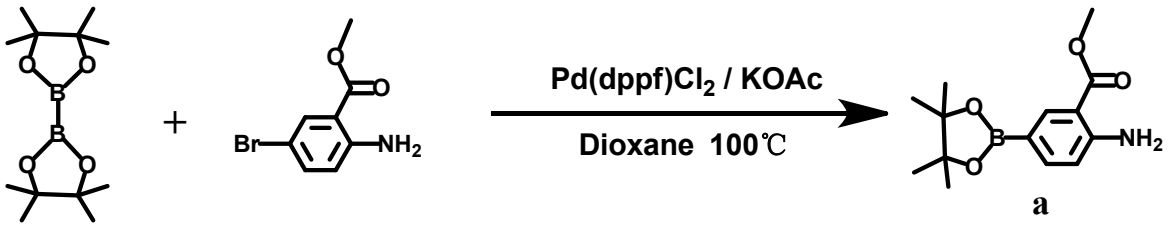

Scheme S2. Synthesis of the phenylboronic acid pinacol ester **a**.

The corresponding phenylboronic acid pinacol ester was prepared according to the literature procedure[5]: To dioxane (20 mL) were added methyl 2-amino-5-bromobenzoate (1.15 g, 5.0

mmol), bis(pinacolato)diboron (1.27g, 5.0 mmol) and potassium acetate (1.47 g, 15 mmol). The mixture was purged with argon flow for 30 min, and Pd(dppf)Cl_2 (200 mg, 0.27 mmol) was then added to the mixture. The reaction was stirred at 100 ℃ for 8 h under argon. Once cooled down to room temperature, the reaction was diluted with CH_2Cl_2 (50 mL). The organic phase was then washed with H_2O (400 mL) and saturated NaCl solution (200 mL). After dried over Na_2SO_4, the organic solvent was removed in vacuo. The crude product was purified via column chromatography (petroleum ether : ethyl acetate = 20 : 1) to yield a white product **a** (803 mg, 2.90 mmol, 58 %). ^{1}H NMR (400 MHz, $CDCl_3$, δ): 8.31 (d, J = 1.27 Hz, 1H), 7.65 (m, J = 8.25, 1.32 Hz, 1H), 6.61 (d, J = 8.26 Hz, 1H), 5.95 (s, 2H), 3.84 (s, 3H), 1.31 (s, 12H).

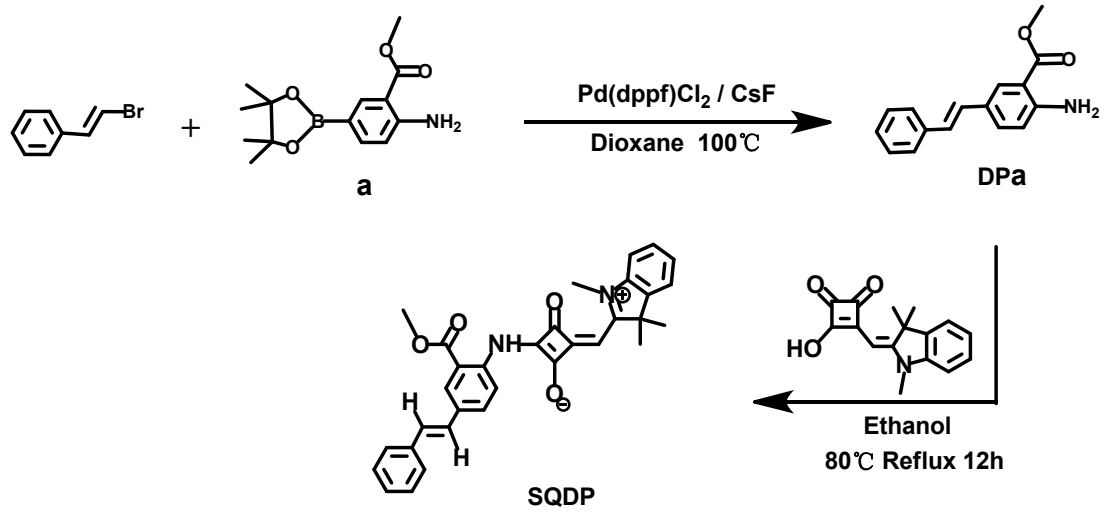

Scheme S3. The overall route for synthesis of **SQDP**.

Synthesis of DPa: To 30 mL dioxane/water (volume ratio is 1:1) were added corresponding phenylboronic acid pinacol ester **a** (1.0 g, 3.6 mmol), (2-bromovinyl)benzene (659 mg, 3.6 mmol) and caesium fluoride (1.47 g, 15 mmol). The mixture was purged with argon flow for 30 min. Pd(dppf)Cl_2 (154 mg, 0.21 mmol) was then added to the mixture. The reaction was stirred at 100 ℃ for 12 h under argon. Once cooled down to room temperature, the reaction was diluted with CH_2Cl_2 (50 mL). The organic phase was then washed with H_2O (400 mL) and saturated NaCl solution (200 mL). After dried over Na_2SO_4, the organic solvent was removed in vacuo. The crude product was purified via column chromatography (petroleum ether : ethyl acetate = 20 : 1) to yield pale yellow product **DPa** (477 mg, 1.87 mmol, 52 %). ^{1}H NMR (400 MHz, $CDCl_3$, δ): 7.97 (s,

1H), 7.47 (m, J = 14.14, 8.20 Hz, 3H), 7.32 (t, J = 7.47 Hz, 2H), 7.20 (t, J = 7.40 Hz, 1H), 6.95 (q, J = 16.31 Hz, 2H), 6.67 (d, J = 8.52 Hz, 1H), 5.85-5.15 (s, 2H), 3.89 (s, 3H).

Synthesis of SQDP: A procedure similar to the synthesis of **SQP** was followed. To a 50 mL round bottom flask was added semisquaraine (538 mg, 2 mmol) and **DPa** (506 mg, 2 mmol) in 20 mL distilled EtOH. After reflux for 12 h at 80 ℃, the mixture was cooled to room temperature, the organic solvent was removed in vacuo. The crude product was then purified via column chromatography (CH_2Cl_2 : CH_3OH = 100 : 1) to yield dark red product **SQDP** (685 mg, 1.36 mmol, 68%). ^{1}H NMR (400 MHz, $CDCl_3$, δ): 11.64 (s, 1H), 8.79 (d, J = 8.69 Hz, 1H), 8.12 (d, J = 1.76 Hz, 1H) 7.78 (m, J = 8.78, 1.79 Hz, 1H), 7.50 (d, J = 7.36 Hz, 2H), 7.35 (t, J = 7.70 Hz, 4H), 7.26 (d, J = 7.31 Hz, 1H), 7.18 (t, J = 7.32 Hz, 1H), 7.05 (m, J = 13.23, 6.10 Hz, 3H), 5.94 (s, 1H), 3.98 (s, 3H), 3.58 (s, 3H), 1.75 (s, 6H). ^{13}C NMR (100 MHz, $CDCl_3$, δ): 172.78, 168.02, 138.95, 136.93, 132.95, 132.44, 129.10, 129.08, 128.71, 127.94, 127.84, 126.91, 126.53, 124.41, 122.29, 121.75, 115.64, 109.62, 52.70, 49.59, 26.99. HRMS m/z: [**SQDP+H**]$^+$ calcd. for $C_{32}H_{28}N_2O_4$, 505.2122; found, 505.2127.

3.3 Synthesis of SQHTPE

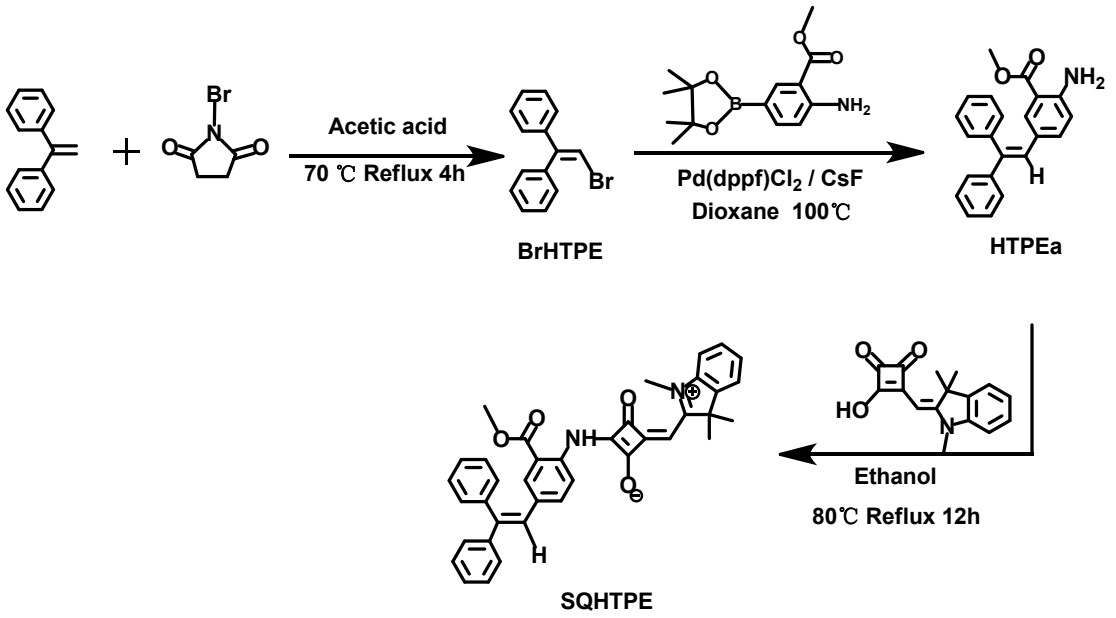

Scheme S4. The overall route for synthesis of **SQHTPE.**

Synthesis of BrHTPE: The corresponding BrHTPE was prepared according to the literature procedure[6]. To a suspension of 1,1-diphenylethene (900mg, 5 mmol) in AcOH (25 mL) was

added N-bromosuccinimide (NBS, 890mg, 5mmol). The resulting mixture was stirred at 70 ℃ for 4 h. After cooling down to room temperature naturally, the reaction was neutralized by slowly adding NaOH/$NaHCO_3$ (1:1) and extracted with EtOAc (3 x 10 mL). The combined organic layers were dried over $MgSO_4$ and concentrated under reduced pressure. The residue was purified by silica gel flash chromatography (petroleum ether : ethyl acetate = 100:1) to afford the corresponding product **BrHTPE** (1.23 g, 4.75 mmol, 95%). ^{1}H NMR (400 MHz, $CDCl_3$, δ): 7.47 (m, 8H), 7.38-7.27 (m, 2H), 6.90 (d, J = 5.54 Hz, 1H).

Synthesis of HTPEa: To 30 mL dioxane/water (volume ratio is 1:1) were added corresponding phenylboronic acid pinacol ester **a** (1.0 g, 3.6 mmol), **BrHTPE** (932 mg, 3.6 mmol) and caesium fluoride (1.47 g, 15 mmol). The mixture was purged with argon flow for 30 min. Pd(dppf)Cl_2 (150 mg, 0.21 mmol) was then added to the mixture. The reaction was stirred at 100 ℃ for 12 h under argon. Once cooled down to room temperature, the reaction was diluted with CH_2Cl_2 (50 mL). The organic phase was then washed with H_2O (400 mL) and saturated NaCl solution (200 mL). After dried over Na_2SO_4, the organic solvent was removed in vacuo. The crude product was purified via column chromatography (petroleum ether : ethyl acetate = 20 : 1) to yield pale yellow product **HTPEa** (592 mg, 1.8 mmol, 50 %). ^{1}H NMR (400 MHz, $CDCl_3$, δ): 7.65 (d, J = 1.59 Hz, 1H), 7.44-7.24 (m, 8H), 7.22 (d, J = 7.48 Hz, 2H), 6.90-6.78 (m, 2H), 6.35 (d, J = 8.62 Hz, 1H), 5.50 (s, 2H), 3.78 (s, 3H).

Synthesis of SQHTPE: A procedure similar to the synthesis of **SQP** was followed. To a 50 mL round bottom flask was added semisquaraine (538 mg, 2 mmol) and **HTPEa** (658 mg, 2 mmol) in 20 mL distilled EtOH. After reflux for 12 h at 80℃, the mixture was cooled to room temperature, the organic solvent was removed in vacuo. The crude product was then purified via column chromatography (CH_2Cl_2 : CH_3OH = 100 : 1) to yield red product **SQHTPE** (731 mg, 1.26 mmol, 63%). ^{1}H NMR (400 MHz, $CDCl_3$, δ): 11.59 (s, 1H), 8.50 (d, J = 8.71 Hz, 1H), 7.69 (d, J = 1.57 Hz, 1H), 7.24 (m, J = 14.91, 13.78, 11.64, 6.49 Hz, 14H), 7.02 (d, J = 7.84 Hz, 1H), 6.91 (s, 1H), 5.90 (s, 1H), 3.82 (s, 3H), 3.57 (s, 3H), 1.72 (s, 6H). ^{13}C NMR (100 MHz, $CDCl_3$, δ): 172.64, 168.00, 143.28, 142.82, 139.84, 138.08, 135.57, 133.05, 132.36, 130.06, 128.96, 128.23, 127.93, 127.69, 127.46, 126.20, 124.36, 122.27, 120.88, 115.07, 109.57, 52.38, 49.51, 26.99. HRMS m/z: [**SQHTPE+H**]$^+$ calcd. for $C_{38}H_{32}N_2O_4$, 581.2435; found, 581.2438.

3.4 Synthesis of SQTPE

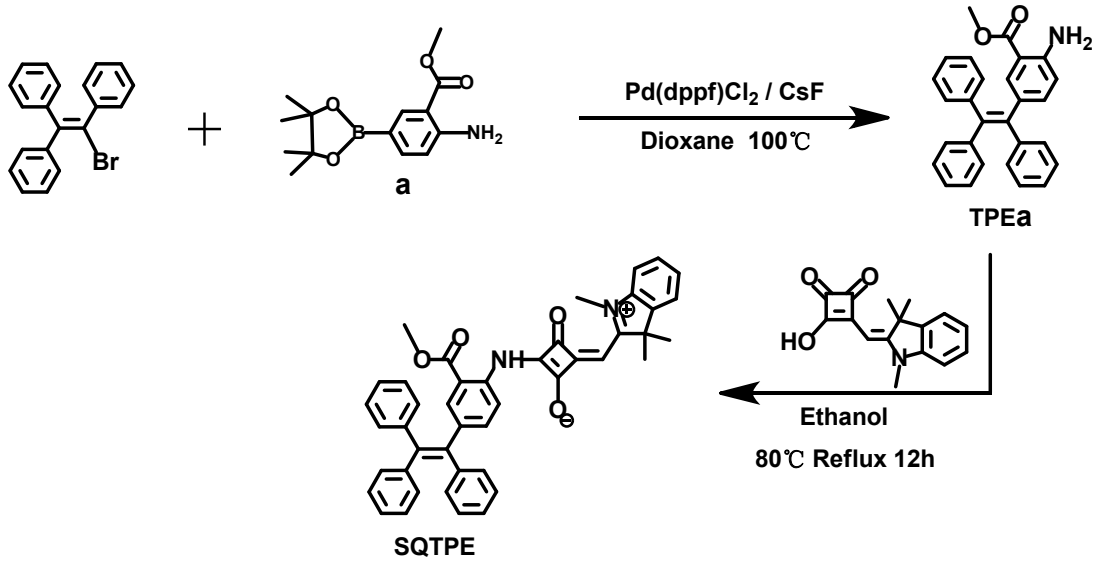

Scheme S5. The overall route for synthesis of **SQTPE**

Synthesis of TPEa: To 30 mL dioxane/water (volume ratio is 1:1) were added corresponding phenylboronic acid pinacol ester **a** (1.0 g, 3.6 mmol), Bromotriphenylethylene (1.2 g, 3.6 mmol) and caesium fluoride (1.47 g, 15 mmol). The mixture was purged with argon flow for 30 min. $Pd(dppf)Cl_2$ (150 mg, 0.21 mmol) was then added to the mixture. The reaction was stirred at 100 ℃ for 12 h under argon. Once cooled down to room temperature, the reaction was diluted with CH_2Cl_2 (50 mL). The organic phase was then washed with H_2O (400 mL) and saturated NaCl solution (200 mL). After dried over Na_2SO_4, the organic solvent was removed in vacuo. The crude product was purified via column chromatography (petroleum ether : ethyl acetate = 20 : 1) to yield white product **TPEa** (891 mg, 2.20 mmol, 61 %).^{1}H NMR (400 MHz, $CDCl_3$, δ): 7.48 (s, 1H), 7.15-6.94 (m, 15H), 6.90 (d, J = 8.16 Hz, 1H), 6.38 (d, J = 8.52 Hz, 1H), 5.71 (s, 2H), 3.70 (s, 3H).

Synthesis of SQTPE: A procedure similar to the synthesis of **SQP** was followed. To a 50 mL round bottom flask was added semisquaraine (538 mg, 2 mmol) and **TPEa** (810 mg, 2 mmol) in 20 mL distilled EtOH. After reflux for 12 h at 80℃, the mixture was cooled to room temperature, the organic solvent was removed in vacuo. The crude product was then purified via column chromatography (CH_2Cl_2: CH_3OH = 100 : 1) to yield red product **SQTPE** (854 mg, 1.30mmol, 65%). ^{1}H NMR (400 MHz, $CDCl_3$, δ): 11.60 (s, 1H), 8.51 (d, J = 8.62 Hz, 1H), 7.65 (d, J = 1.69 Hz, 1H), 7.37-7.25 (m, 3H), 7.20-7.05 (m, 10H), 7.03 (d, J = 8.95 Hz, 7H), 5.95 (s, 1H), 3.58 (s,

3H), 3.79 (s, 3H), 1.72 (s, 6H); ^{13}C NMR (100 MHz, $CDCl_3$, δ): 172.75, 168.04, 143.28, 143.16, 142.80, 142.02, 139.43, 139.18, 137.98, 137.82, 133.85, 131.29, 131.18, 127.94, 127.84, 127.63, 126.81, 126.72, 126.57, 124.37, 122.25, 120.69, 114.95, 109.58, 52.36, 49.53, 26.97. HRMS m/z: [**SQTPE+H**]$^+$ calcd. for $C_{44}H_{36}N_2O_4$, 657.2748; found, 657.2750.

4 Spectroscopic data in solution

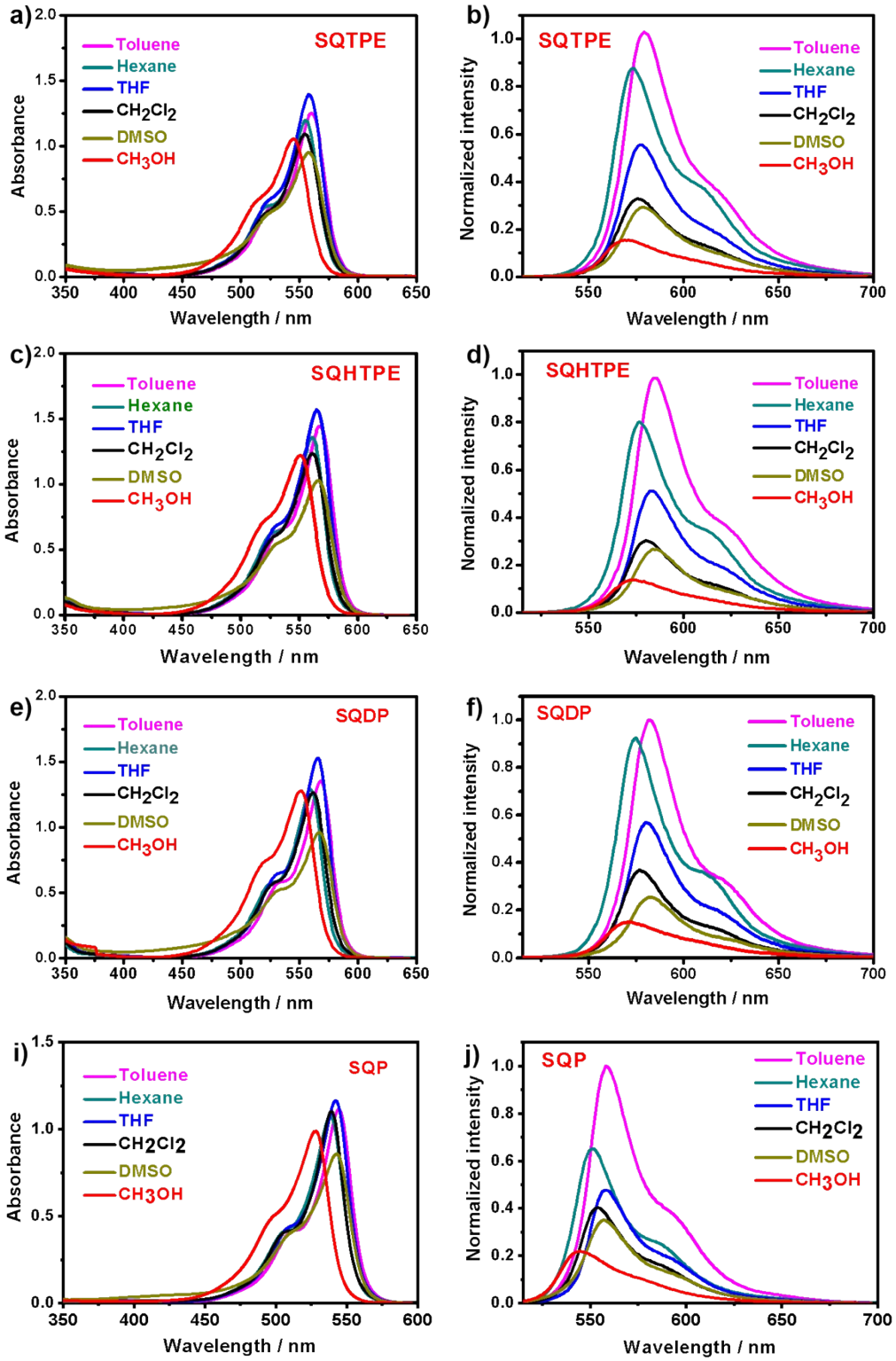

Figure S4. Absorption (left) and emission (right) spectra of a, b) **SQTPE**, c, d) **SQHTPE** e, f) **SQDP** and i, j) **SQP** in various solvents at room temperature (10 μM, λ_{ex} = 500 nm).

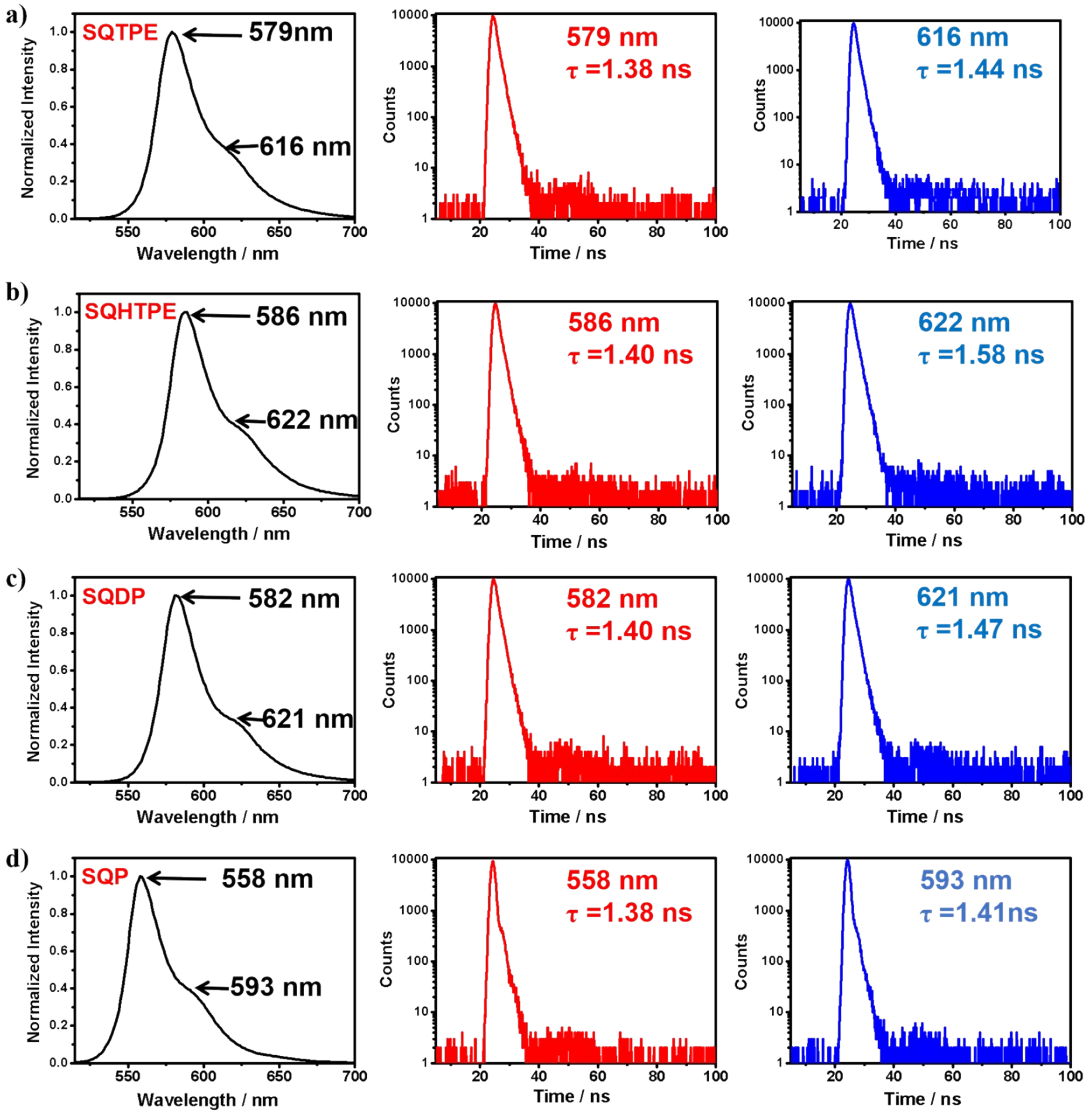

Figure S5. Lifetime decay profiles of target a) **SQTPE** b) **SQHTPE** c) **SQDP** d) **SQP** in toluene (10 μM) at room temperature.

Table S2. The photophysical data for luminogens in solution (10 μM) and solid state at 298K.

Condition		λ_{abs} [nm]	λ_{em}[a)] [nm]	Φ_{PL}[b)] %	τ_f[c)] [ns]	X^2	k_f[d)] [10^9 s^{-1}]	k_{nr}[e)] [10^9 s^{-1}]
SQTPE	Toluene	532/560	579/616	26.9	1.38/1.44	0.99/1.01	0.19/0.17	0.53/0.46
	Hexane	525/555	573/610	22.3	1.37/1.40	1.02/0.99	0.16/0.16	0.57/0.56
	THF	531/558	577/614	14.1	1.41/1.46	0.99/0.99	0.09/0.10	0.57/0.59
	CH_2Cl_2	526/555	576/608	11.8	1.36/1.42	0.99/1.00	0.08/0.08	0.58/0.61
	DMSO	532/558	580/617	10.2	1.44/1.48	0.99/0.99	0.07/0.07	0.62/0.61
	CH_3OH	520	569	3.3	1.50	1.01	0.02	0.60
SQHTPE	Toluene	537/568	586/622	57.5	1.50/1.58	1.00/1.01	0.41/0.38	0.30/0.28
	Hexane	533/561	577/614	47.4	1.50/1.52	1.01/0.99	0.31/0.32	0.35/0.35
	THF	535/565	583/623	29.8	1.48/1.55	0.99/0.99	0.21/0.20	0.49/0.47
	CH_2Cl_2	529/561	585/619	16.4	1.44/1.54	1.01/1.01	0.11/0.12	0.54/0.60
	DMSO	535/566	584/617	13.3	1.52/1.57	0.99/1.00	0.09/0.08	0.56/0.55
	CH_3OH	522/551	573/605	5.1	1.51/1.53	1.01/0.99	0.03/0.04	0.62/0.70
SQDP	Toluene	536/568	582/621	42.7	1.40/1.47	0.99/1.07	0.35/0.34	0.36/0.34
	Hexane	532/559	575/611	37.2	1.43/1.48	1.01/1.03	0.25/0.26	0.42/0.44
	THF	533/566	580/616	26.8	1.40/1.51	0.99/1.06	0.19/0.18	0.52/0.48
	CH_2Cl_2	530/562	577/614	11.3	1.39/1.47	1.01/0.99	0.08/0.08	0.60/0.65
	DMSO	536/567	582/619	7.2	1.45/1.49	1.01/1.08	0.05/0.02	0.64/0.30
	CH_3OH	523/551	571/600	4.6	1.43/1.52	1.00/0.99	0.03/0.04	0.63/0.93
SQP	Toluene	508/544	558/593	11.3	1.38/1.41	1.01/1.00	0.08/0.08	0.64/0.63
	Hexane	512/538	551/585	7.2	1.39/1.43	1.01/0.97	0.05/0.04	0.58/0.57
	THF	513/542	558/587	4.7	1.42/1.50	0.99/1.01	0.03/0.03	0.67/0.60
	CH_2Cl_2	507/539	554/585	4.3	1.35/1.40	1.01/1.00	0.03/0.03	0.64/0.63
	DMSO	515/543	557/588	3.4	1.39/1.48	1.01/1.02	0.02/0.02	0.69/0.65
	CH_3OH	501/528	544/580	2.3	1.43/1.51	1.02/1.01	0.02/0.01	0.68/0.59

[a)]λ_{ex} = 500 nm; [b)]Measured using an intergrating sphere method; [c)]Measured using a single-photocounting method; [d)]Radiative rate constant ($k_f = \Phi_f/\tau_f$); [e)]Nonradiative rate constant ($k_{nr} = (1-\Phi_f)/\tau_f$).

5 Crystal study

5.1 Crystal data

Table S3. Crystallographic data of **SQTPE**, **SQHTPE**, **SQDP**.

Sample	SQTPE	SQHTPE	SQDP
CCDC	1887512	1950733	1950732
Empirical formula	$C_{44}H_{36}N_2O_4$	$C_{38}H_{32}N_2O_4$	$C_{32}H_{28}N_2O_4$
Formula weight	656.77	580.67	504.58
Temperature	296.15 K	293(2) K	296(2) K
Wavelength	0.71073 Å	0.71073 Å	0.71073 Å
Crystal system, space group	Triclinic, P-1	Orthorhombic, Pca2(1)	Triclinic, P-1
Unit cell dimensions	a = 10.621(4) Å b = 12.212(5) Å c = 15.963(7) Å α = 91.512(6) deg. β = 93.210(6) deg. γ = 109.177(6) deg.	a = 35.3194(17) Å b = 7.1526(3) Å c = 12.1579(6) Å α = 90 deg. β = 90 deg. γ = 90 deg.	a = 7.6852(14) Å b = 12.902(2) Å c = 13.238(2) Å α = 94.434(2) deg. β = 92.097(2) deg. γ = 101.766(2) deg.
Volume	1950.3(14) $Å^3$	3071.4(2) $Å^3$	1279.4(4) $Å^3$
Z, Calculated density	2, 1.118 Mg/m^3	4, 1.256 Mg/m^3	2, 1.310 Mg/m^3
Absorption coefficient	0.072 mm^{-1}	0.082 mm^{-1}	0.087 mm^{-1}
F(000)	692	1224.0	532
Crystal size	0.3 x 0.2 x 0.15 mm	0.4 x 0.2 x 0.02 mm	0.4 x 0.2 x 0.04 mm
Theta range for data collection	2.211 to 25.00 deg.	3.33 to 25.00 deg.	2.33 to 25.00 deg.
Limiting indices	$-12\leq h\leq 12$, $-14\leq k\leq 14$, $-18\leq l\leq 17$	$-42\leq h\leq 42$, $-8\leq k\leq 8$, $-14\leq l\leq 14$	$-9\leqslant h\leqslant 9$, $-15\leqslant k\leqslant 15$, $-15\leqslant l\leqslant 15$
Reflections collected/unique	14461/6830 [R(int) = 0.0448]	25900/5394 [R(int) = 0.0333]	9068/4430 [R(int) = 0.0512]
Completeness to theta= 25.00	99.4 %	99.8 %	98.0 %
Absorption correction	None	None	None
Refinement method	Full-matrix least-squares on F^2	Full-matrix least-squares on F^2	Full-matrix least-squares on F^2
Data / restraints / parameters	6830/ 0 / 451	5394/ 1 / 401	4430 / 0 / 347
Goodness-of-fit on F^2	0.942	1.037	0.851
Final R indices [I>2sigma(I)]	$R_1 = 0.0559$, $wR_2 = 0.1312$	$R_1 = 0.0436$, $wR_2 = 0.1342$	R1 = 0.0720, wR2 = 0.1501

R indices (all data)	$R_1 = 0.1249$, $wR_2 = 0.1606$	$R_1 = 0.0496$, $wR_2 = 0.1394$	R1 = 0.1637, wR2 = 0.1722

5.2 Crystal structure analysis

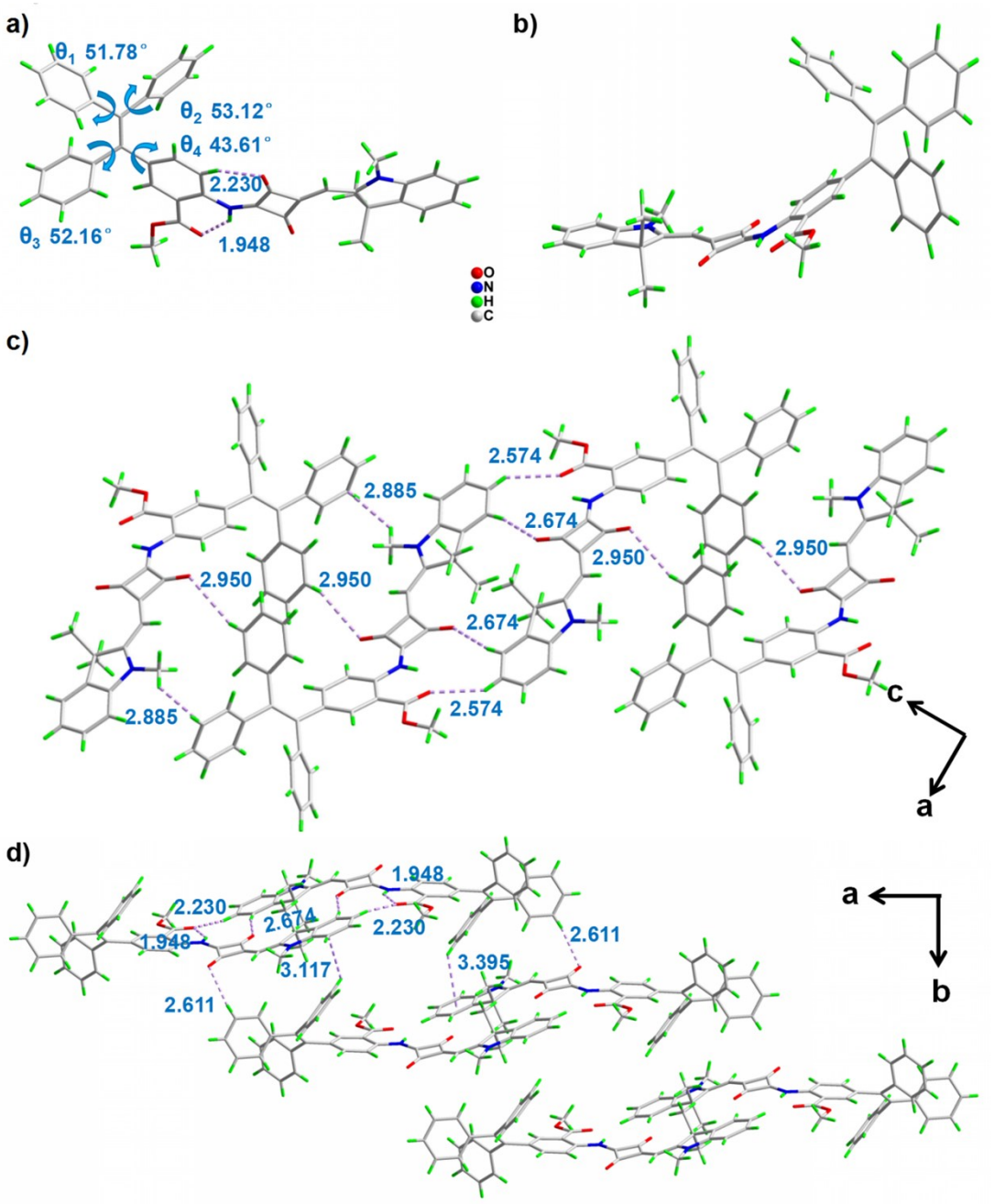

Figure S6. The molecular structures and packing mode in the **SQTPE** crystal. a) The molecular conformation and intramolecular hydrogen-bnding interactions. b) The dihedral angles between vinyl bond and phenyl rotors. Intermolecular hydrogen-bonding and Ar-H···π interactions between adjacent **SQTPE** molecules along c) a, c-axis and d) b-axis.

SQTPE crystal belonged to a triclinic crystal system and crystallized in the space group of P-1 with two **SQTPE** molecules in one unit cell taking the parameters of a = 10.621(4), b = 12.212(5) and c = 15.963(7) Å. It is noteworthy that multiple intra/intermolecular hydrogen bonding served to the construction of the crystalline **SQTPE** without any π stacking. In the whole **SQTPE** molecule, the SQ segment was distorted in spite of there existed two types of strong intramolecular C=O···H hydrogen bonding (Figure S6a-b). One was 2.230 Å between Ar-H and carbonyl in four-member ring, and another one was 1.949 Å between N-H and adjacent methyl esters. And this vividly molecular distortion can be ascribed to multiple intermolecular hydrogen bonding interactions. As compared to TPE molecule[7], the dihedral angles between vinyl bond and phenyl rotors exhibited obvious change for θ_1 from 56.74° to 51.67°, θ_2 from 45.66° to 53.12°, θ_3 from 46.18° to 52.16° and and θ_4 from 48.43° to 43.61°, respectively, in **SQTPE** molecule. These remarkable changes supported the enhanced rigidity of the whole **SQTPE** molecule in crystalline state. As shown in Figure S6c, two types of moderate C=O···H hydrogen bonding between Ar-H and carbonyl in four-member ring were observed in 2.950 Å and 2.674 Å, and a C=O···H hydrogen bonding in 2.574 Å between Ar-H and carbonyl in methyl esters as well as an H···π interaction in 2.801 Å between phenyl group and C-H in methyl esters were also observed along the a and c axis. Along the b axis, there also existed multiple moderate to strong hydrogen bonding interactions between adjacent **SQTPE** molecules. As such, this special packing mode dominated by multiple intermolecular C-H···O and C-H···π interactions, as well as no phenyl group was in free, would well support the fact that **SQTPE** exhibited most efficient emission with Φ_{PL} = 73.1% in crystalline state.

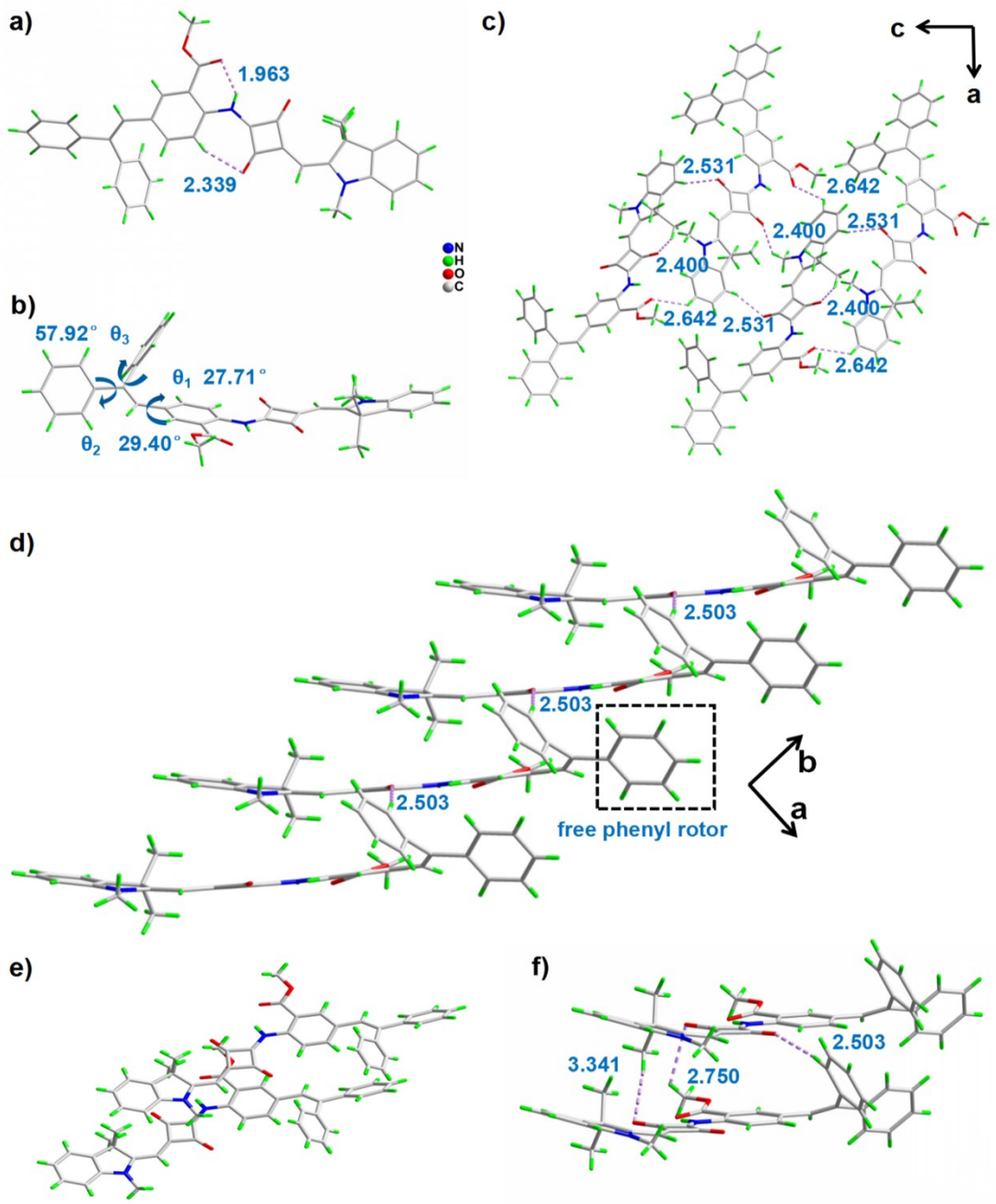

Figure S7. The molecular structure and packing mode in the **SQHTPE** crystal. a) The molecular conformation and intramolecular hydrogen-bnding interactions in front view and b) The dihedral angles between vinyl bond and phenyl rotors in side view. c) Multiple intermolecular hydrogen-bonding interactions between adjacent **SQHTPE** molecules along c-axis. d) Continuous intermolecular interactions along b-axis including e) no π-π interactions and f) two types of intermolecular hydrogen bonding interactions.

SQHTPE crystal belonged to an orthorhombic crystal system and crystallized in the space group of Pca2(1) with four **SQHTPE** molecules in one unit cell taking the parameters of a = 35.3194(17), b = 7.1526(3) and c = 12.1579(6) Å. Similarly to **SQTPE**, two types of strong intramolecular C=O···H hydrogen bonding were observed in the **SQHTPE** molecule (Figure S7a). One was 2.339 Å between Ar-H and carbonyl in four-member ring, and another one was 1.963 Å between N-H and ortho methyl ester. Meanwhile, the dihedral angles between vinyl bond and phenyl rotors were detected as θ_1 = 57.92°, θ_2 = 29.40° and θ_2 = 27.71° in **SQHTPE** molecule (Figure S8b), ensuring its twisting configuration. As shown in Figure 7c, three types of moderate hydrogen bonding interactions were observed between adjacent **SQHTPE** molecules, which was in a "stair-like" type rising along the a and c-axis. One was 2.642 Å interaction in C=O···H between the oxygen atom of methyl ester and hydrogen atom of phenyl rotor, the second one was 2.531 Å interaction in Ar-H···O between the oxygen atom of four-membered ring and hydrogen atom of phenyl rotor, and the final one was 2.400 Å interaction in C-H···O between the hydrogen atom of methyl and oxygen atom of four-membered ring (Figure S7c). While along the b axis, there also exhibited two types of intermolecular hyrdrogen bonding interactions in 3.341 Å/2.503 Å between the oxygen atom of central four-member ring and hydrogen atom of methyl/phenyl group, rather than π-π interactions (Figure S7d-f). It is noteworthy that the cis phenyl rotor was in free without any interactions even though it was in crystalline state (Figure S7d), which would consume certain exciton energies leading to a moderate emission intensity with Φ_{PL} = 51.2% in **SQHTPE** crystals.

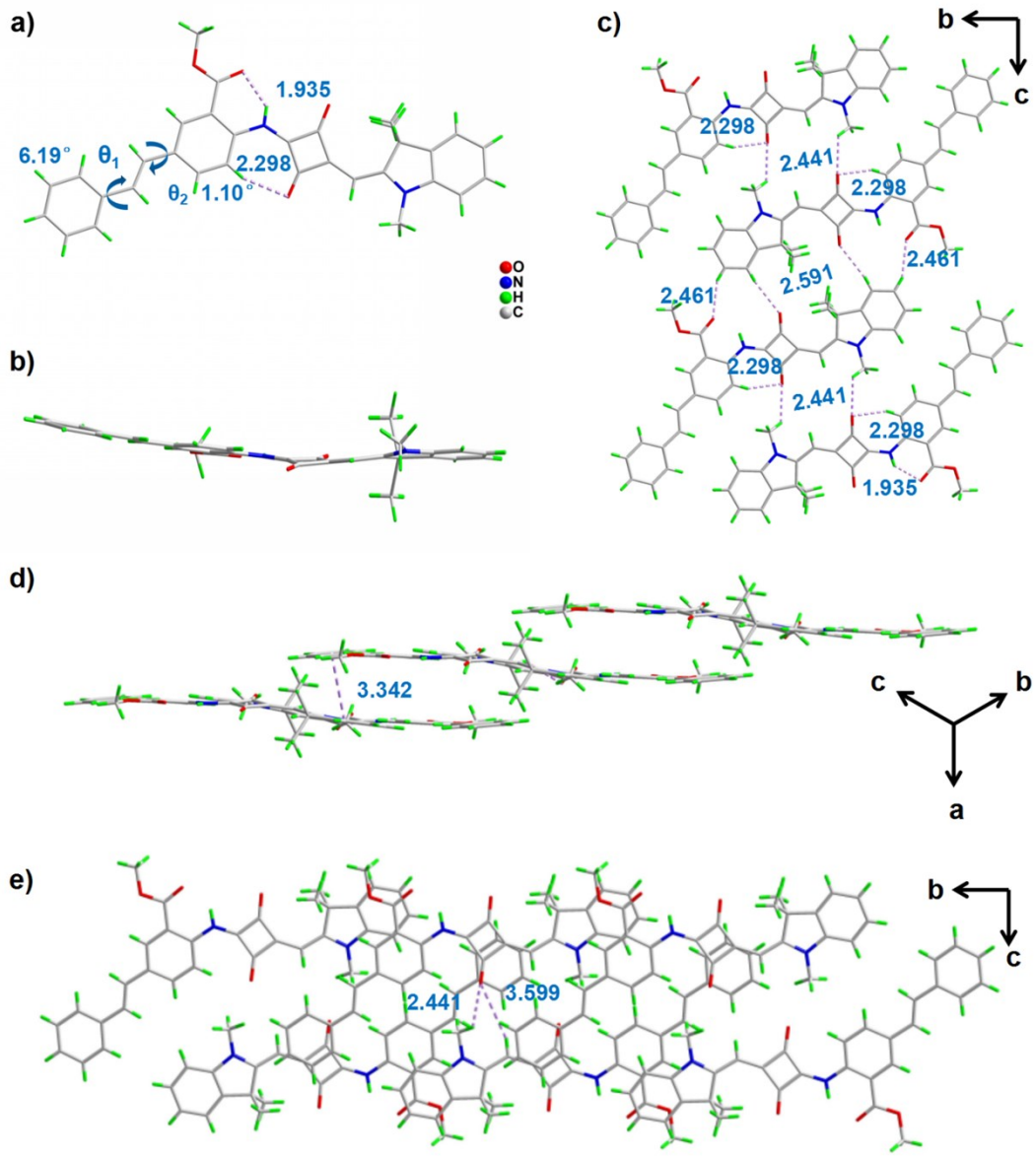

Figure S8. The molecular structure and packing mode in the **SQDP** crystal. The molecular conformation and intramolecular hydrogen-bnding interactions in a) front view and b) side view. c) Multiple intermolecular hydrogen-bonding interactions between adjacent **SQDP** molecules. Continuous intermolecular π-π interactions in d) side view and e) front view along a-axis.

SQDP crystal belonged to a triclinic crystal system and crystallized in the space group of P-1 with two **SQDP** molecules in one unit cell taking the parameters of a = 7.685(14), b = 12.902(10) and c = 13.238(4) Å. The whole **SQDP** molecule was nearly plane due to two types of strong intramolecular C=O···H hydrogen bonding (Figure S8a-b). One was 2.298 Å between Ar-H and carbonyl in four-member ring, and another one was 1.935 Å between N-H and ortho methyl ester.

Meanwhile, 2.441 Å interactions in C-H···O between hydrogen atom of methyl and oxygen atom of four-membered ring, accompanying pairwise 2.461 and 2.591 Å intermolecular interactions in C=O···H between Ar-H and oxygen atom of methyl ester and four-membered ring, respectively, were observed in adjacent **SQDP** molecules (Figure S8c). Along the a axis, there exhibited continuous intermolecular weak π-π interactions in 3.342 Å between central four-member ring and phenyl group at the distal end of the **SQDP**, resulting into antiparallel packing ways between adjacent **SQDP** molecules (Figure S8d-e). This larger conjugation and weaker π stacking would result into the relatively efficient emission of **SQDP** with Φ_{PL} = 40.5% in crystalline state.

5.3 Preparations and characterizations of crystalline assemblies

All the microstructures were prepared via a liquid phase self-assembly method. Taking **SQTPE** as an example: 50 mg **SQTPE** was completely dissolved in the 4 mL refluxing CH_2Cl_2/Hexane (volume ratio is 1:3) solution with vigorous sonication for 15 min. After cooling and aging in closed tubes at room temperature for 30 min, the **SQTPE** assemblies with suitable dimensions were formed in the solutions. These microstructures were then used to prepare samples for further characterizations.

As shown, photoluminescence (PL) microscopy and scanning electron microscopy (SEM) images revealed that the assembly of **SQP** and **SQHTPE** molecules both yielded thin nanosheets with edge lengths of about 60 to 200 μm and thicknesses around several micrometers, while the **SQDP** and **SQTPE** nanoblocks were about 20-30 μm in width and 20-50 μm in length as well as thicknesses around several to ten micrometers (Figure S9). Furthermore, power X-ray diffraction (PXRD) patterns of these pristine crystalline powders showed sharp and intense peaks, indicating good microcrystalline structures. The simulated XRD patterns of **SQTPE**, **SQHTPE** and **SQDP** crystals turned out to be coincided with that of their crystalline assemblies (Figure S10), suggesting the same molecular packing modes. Thermogravimetric analysis (TGA) experiments revealed that these microstructures were stable until ≈ 270 ℃ with the exception of **SQP** assemblies (Figure S11b-d), which was stable until 284 ℃ (Figure S11a). Obviously, those results revealed that relatively strong intermolecular π-π interactions existed in crystalline **SQP** in view of its planar configuration.

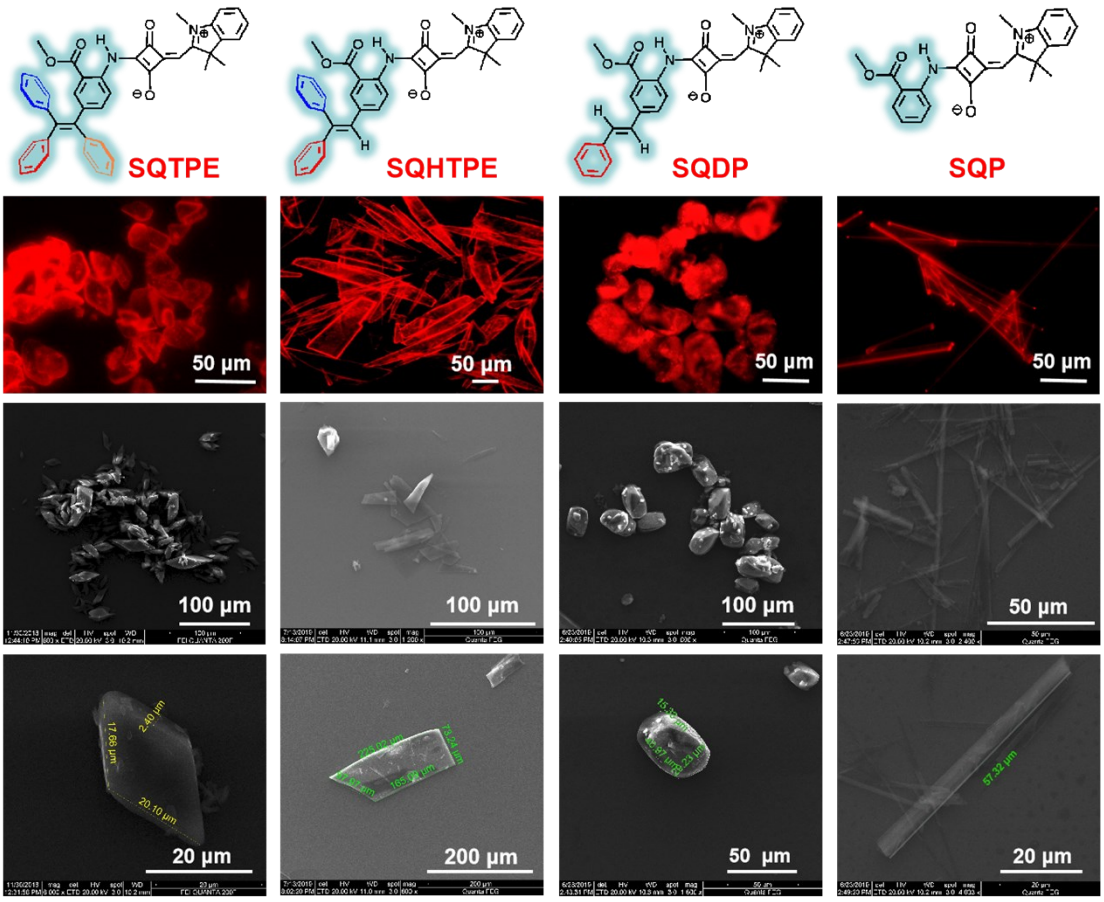

Figure S9. Structures of **SQTPE**, **SQHTPE**, **SQDP**, and **SQP** and their corresponding photographs in crystalline assemblies taken under 365 nm UV illumination and SEM.

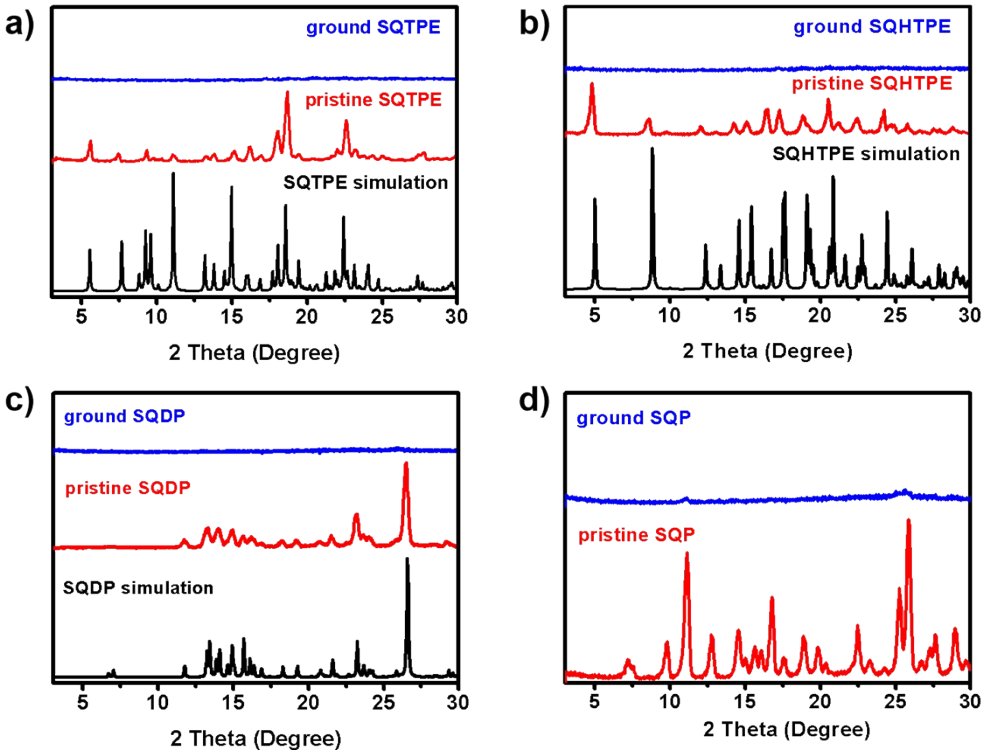

Figure S10. The XRD patterns of a) **SQTPE**, b) **SQHTPE**, c) **SQDP** and d) **SQP** assemblies in pristine and ground state as well as the simulated XRD patterns of corresponding crystals.

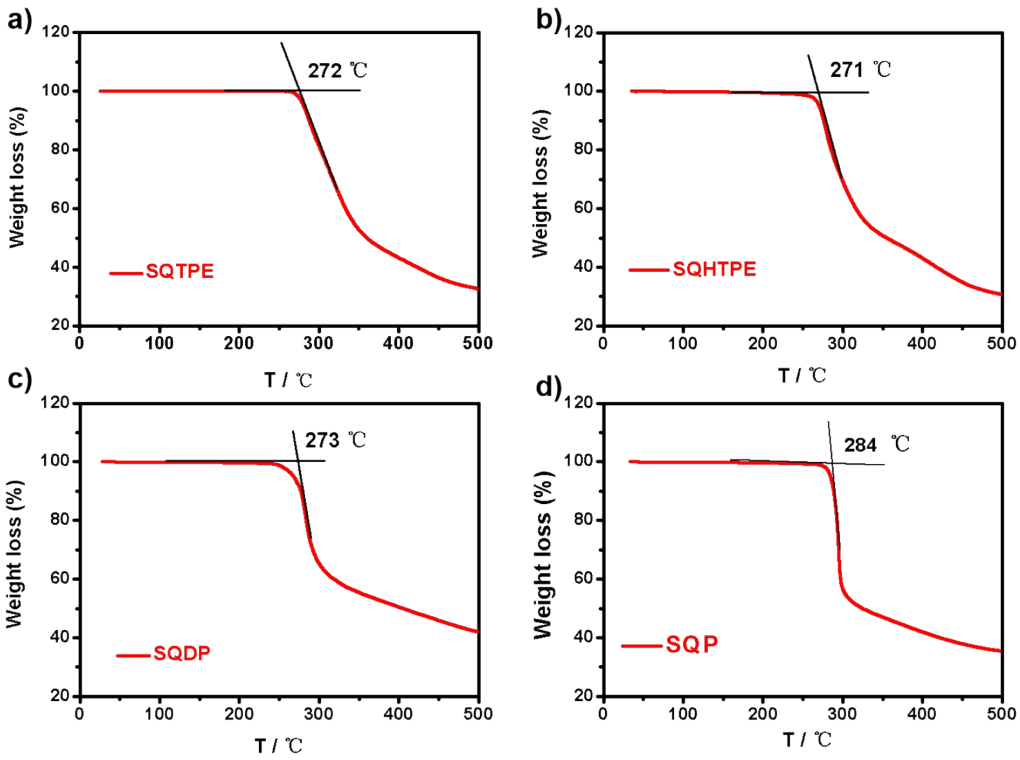

Figure S11. TGA curves of pristine a) **SQTPE**, b) **SQHTPE**, c) **SQDP** and d) **SQP** assemblies at heating rate of 5 ℃ min^{-1} under N_2 atmosphere.

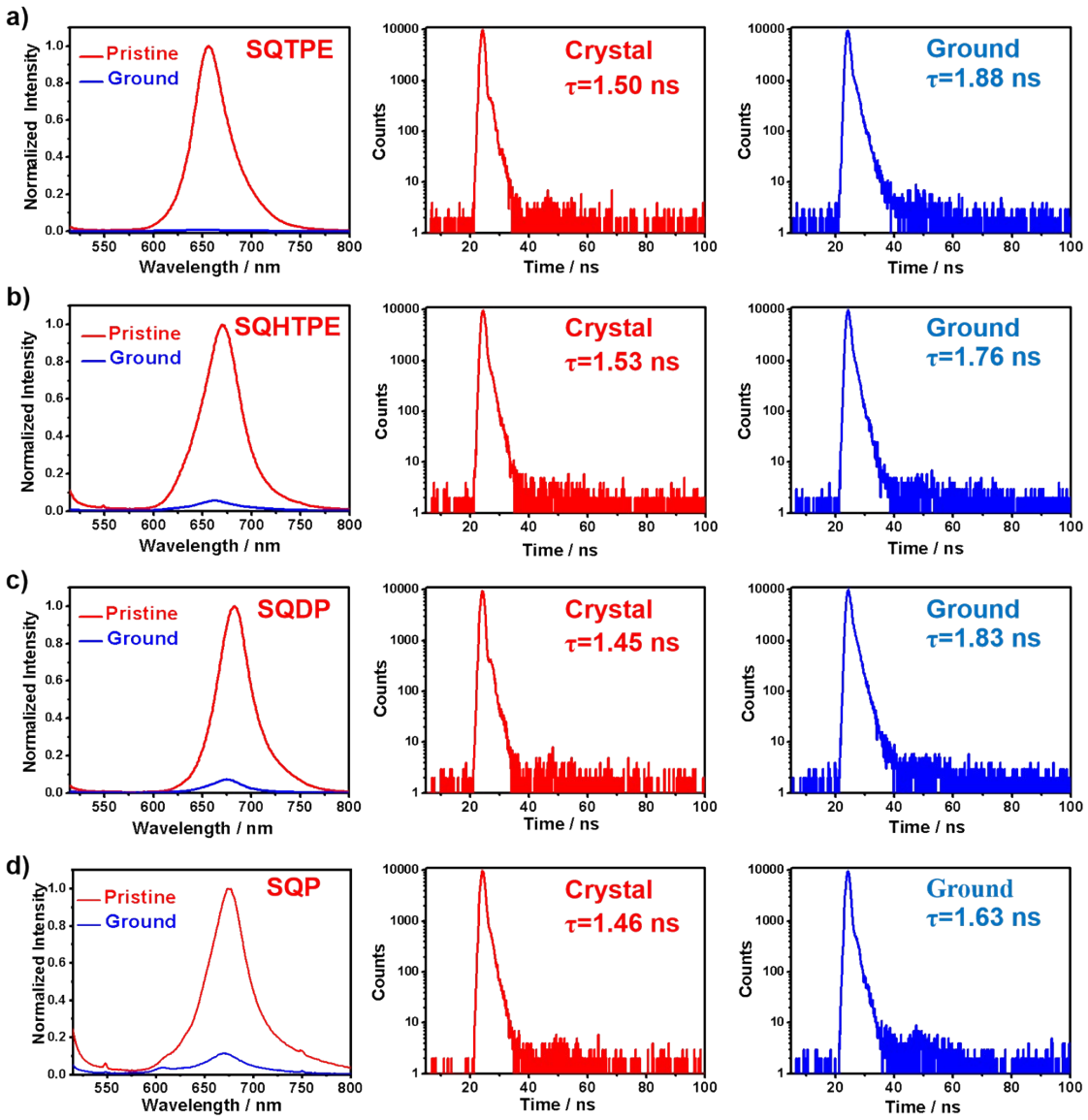

Figure S12. The emission spectra Lifetime and their corresponding decay profiles of a) **SQTPE**, b) **SQHTPE**, c) **SQDP** and d) **SQP** assemblies in different condition at room temperature.

Table S4. The photophysical data for **SQTPE**, **SQHTPE**, **SQDP**, **SQP** assemblies in different condition at 298K.

Crystalline condition		λ_{abs} [nm]	λ_{em}[a)] [nm]	Φ_{PL}[b)] %	τ_f[c)] [ns]	X^2	k_f[d)] [10^9 s^{-1}]	k_{nr}[e)] [10^9 s^{-1}]
SQTPE	pristine	---	656	73.1	1.50	1.04	0.49	0.18
	Ground	---	649	< 1	1.88	1.00	---	---
SQHTPE	pristine	---	670	51.2	1.53	1.01	0.33	0.32
	Ground	---	662	< 1	1.76	0.99	---	---
SQDP	pristine	---	682	40.5	1.45	0.99	0.28	0.41
	Ground	---	675	< 1	1.83	1.00	---	---
SQP	pristine	---	675	8.1	1.46	0.99	0.06	0.63
	Ground	---	674	<1	1.63	1.00	---	---

[a)]λ_{ex} = 500 nm; [b)]Measured using an intergrating sphere method; [c)]Measured using a single-photocounting method; [d)]Radiative rate constant ($k_f = \Phi_f/\tau_f$); [e)]Nonradiative rate constant ($k_{nr} = (1-\Phi_f)/\tau_f$).

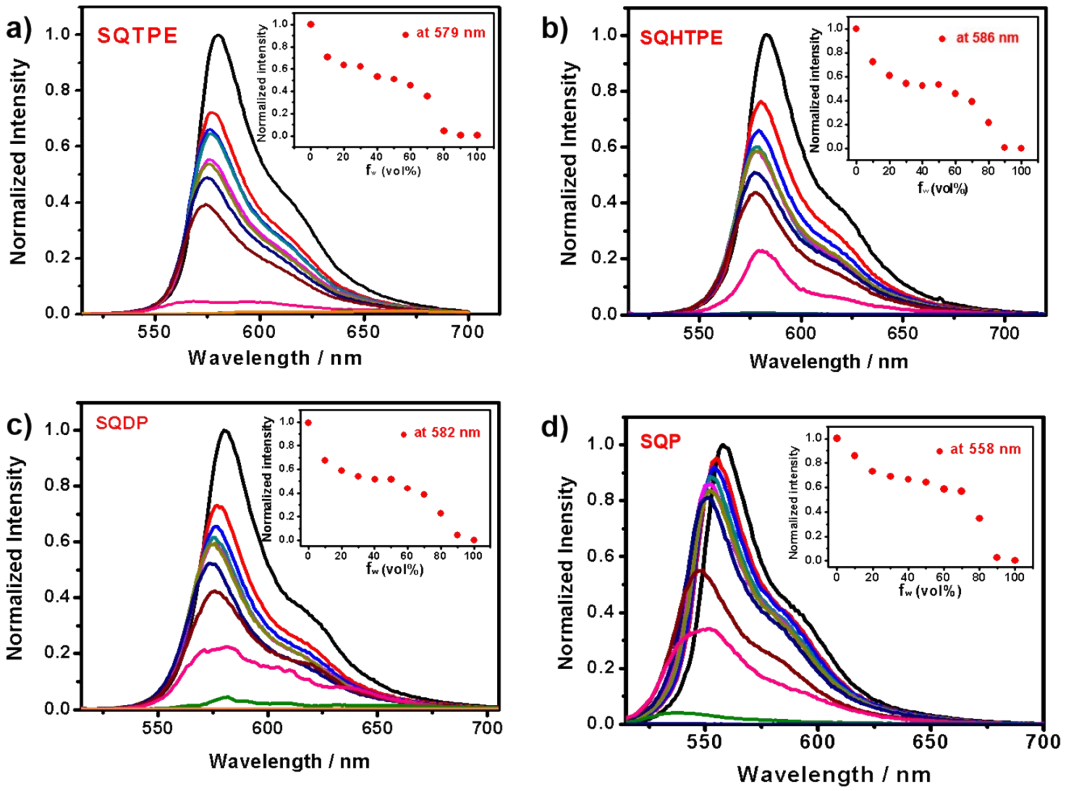

Figure S13. Emission spectra of a) **SQTPE**, b) **SQHTPE**, c) **SQDP** and d) **SQP** (10 μM) in THF solution with different fractions of water (f_w) at room temperature, λ_{ex} = 500 nm.

To study optical properties of these molecules in aggregated state, their emission behaviors in THF solution with different fractions of water (f_w, by volume) were then monitored (Figure S13). When relative low fraction of water was introduced into the THF solution, negligible nanoparticles were observed and the emission intensity of these four compounds decreased gently with all λ_{em} peaks shifted to short wavelength. These ostensible ACQ behaviors can be ascribed to their good solubility in THF and the solvation effect of water similarly to that in protic CH_3OH. Upon f_w over 70%, their emission became much weaker and tiny nanoparticles were observed, indicating all of them exhibited a typical ACQ behavior.

Table S5. The emission data for the reported DSE molecules.

Structure	Emission				DSE shift (nm)	References
	In solution		In solid state			
	λ_{em} (nm)	Φ_{PL}	λ_{em} (nm)	Φ_{PL}		
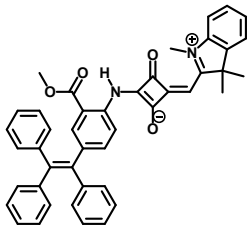	579/616	0.269	656	0.731	77	This work
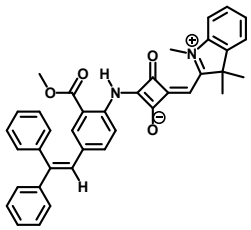	586/622	0.575	670	0.512	84	
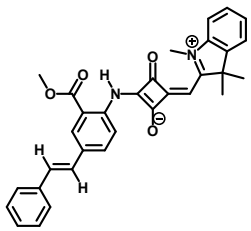	582/621	0.427	682	0.405	100	
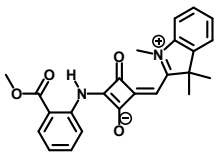	558/593	0.113	675	0.081	117	
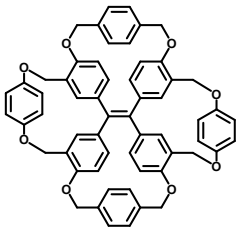	492	0.97	484	0.80	-8	*J. Am. Chem. Soc.* **2016**, 138, 11469-11472.
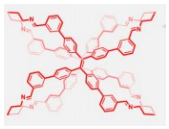	494	0.76	506	0.83	12	*J. Am. Chem. Soc.* **2019**, 141, 4704-4710.
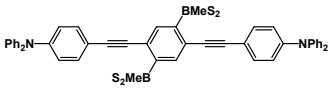	559	0.98	562	0.90	3	*J. Am. Chem. Soc.* **2006**, 128, 15934-15935.

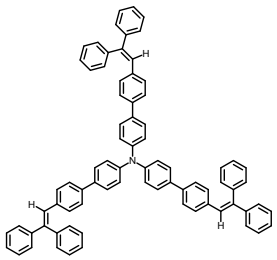	**445**	**0.73**	**455**	**0.55**	**10**	*Adv. Mater.* **2015**, *27*, 4496-4501.
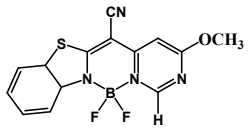	**412**	**0.61**	**484**	**0.20**	**72**	*Dalton Trans*, 45(43), 17274-17280.
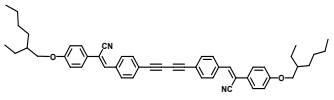	**450**	**0.98**	**500**	**0.40**	**50**	*Angew. Chem. Int. Ed.* **2019**, 58, 11419-11423.
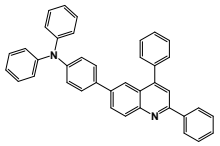	**492**	**0.70**	**481**	**0.48**	**-11**	*ACS Appl. Bio Mater.* **2019**, 2, 3686-3692.
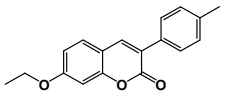	**425**	**0.73**	**450**	**0.98**	**25**	*Dyes and Pigments* **2018**, 149, 73-81.
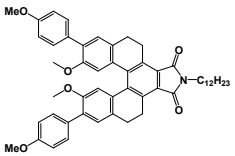	**506**	**0.93**	**518**	**0.62**	**12**	*Chem. Commun.*, ***2014***, 50, 2993-2995.
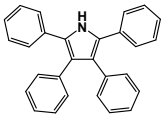	**399**	**0.66**	**403**	**0.74**	**4**	*Chem. Eur. J.* **2018**, 24, 1-7.
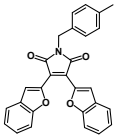	**555**	**0.47**	**630**	**0.46**	**75**	*Chem. Eur. J.* **2018**, 24, 322-326.
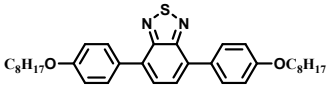	**536**	**1**	**520**	**0.77**	**16**	*Chem. Eur. J.* **2018**, 24, 10383-10389.
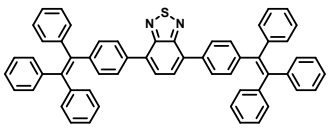	**538**	**0.61**	**539**	**0.89**	**1**	*Chem. Commun.,* **2011**, 47, 8847-8849
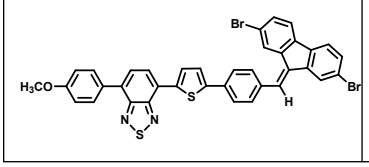	**580**	**0.22**	**596**	**0.20**	**16**	*J. Phys. Chem. C* **2016**, 120, 26556-26568.

6 Cell imaging

6.1 Method

Human umbilical vein endothelial cells (HUVECs, 2-3 × 10^4 mL^{-1}) were plated in petri dishes and cultured in the incubator (37 ℃, 5% CO_2) for 24 h to reach a ~70% confluence. And the cells were fixed by 4% paraformaldehyde then washed twice with PBS and incubated with different concentrations of **SQHTPE** for 30 min at 37 ℃ respectively, washed again. And then stained with DAPI for 30 min at 37 ℃. After washing twice with PBS, the cell samples were subjected to confocal microscopy.

6.2 Stability tests

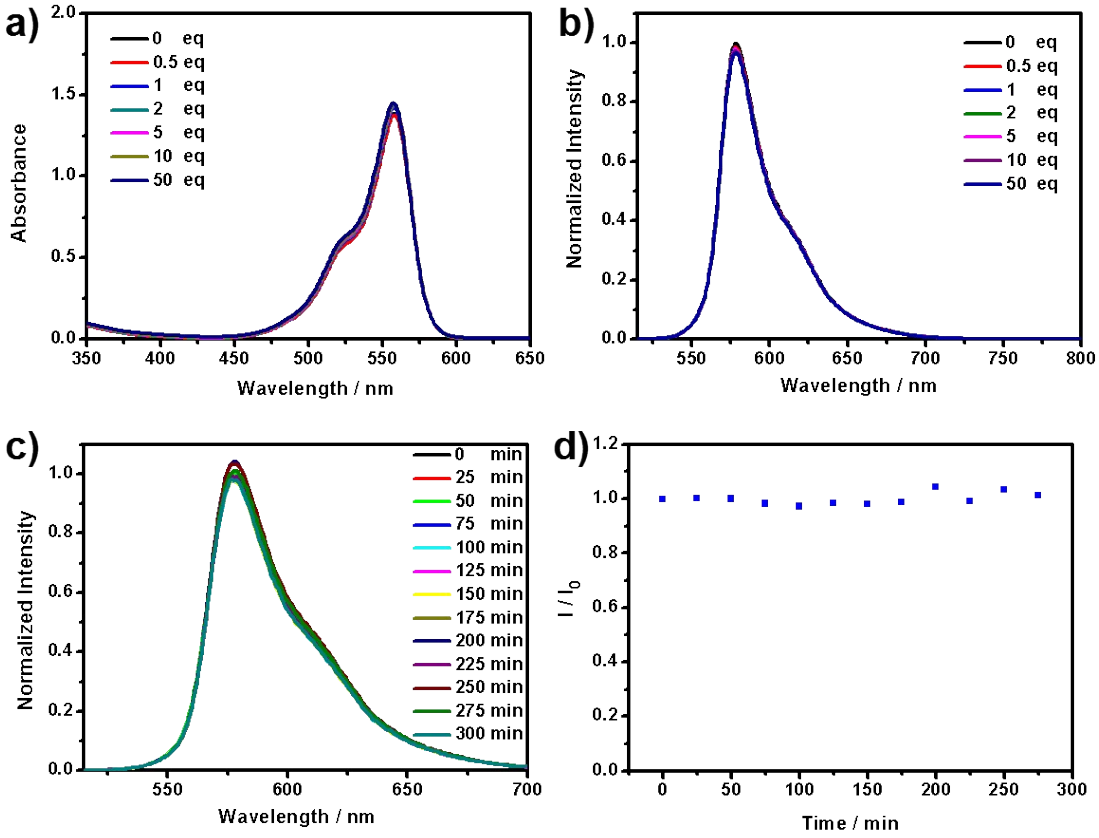

Figure S14. a) Absorption and b) emission spectra of **SQHTPE** (10 μM) in THF with addition of Cys, λ_{ex} = 500 nm. c) emission spectra of **SQHTPE** (10 μM) in CH_2Cl_2 solution under lab light. d) corresponding photostability of **SQHTPE**.

6.3 Cell viability

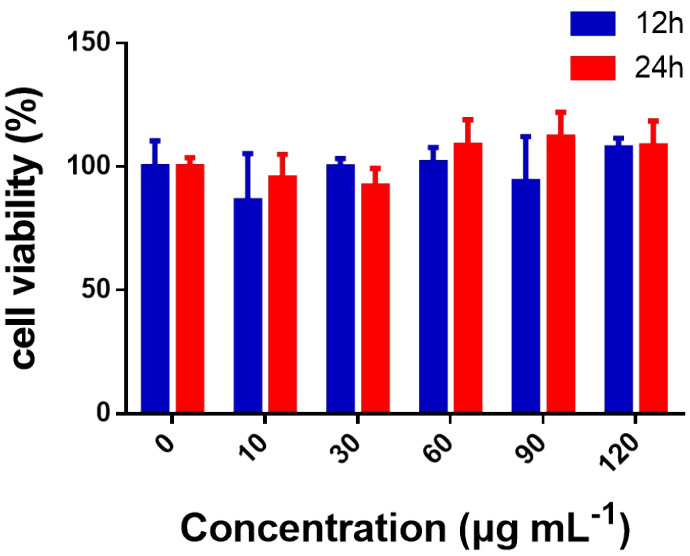

Figure S15. Cell viability of **SQHTPE** with HUVECs for 12 and 24 h (Cell viability was determined by the MTT assay).

7 ^{1}H NMR, ^{13}C NMR and MS spectra

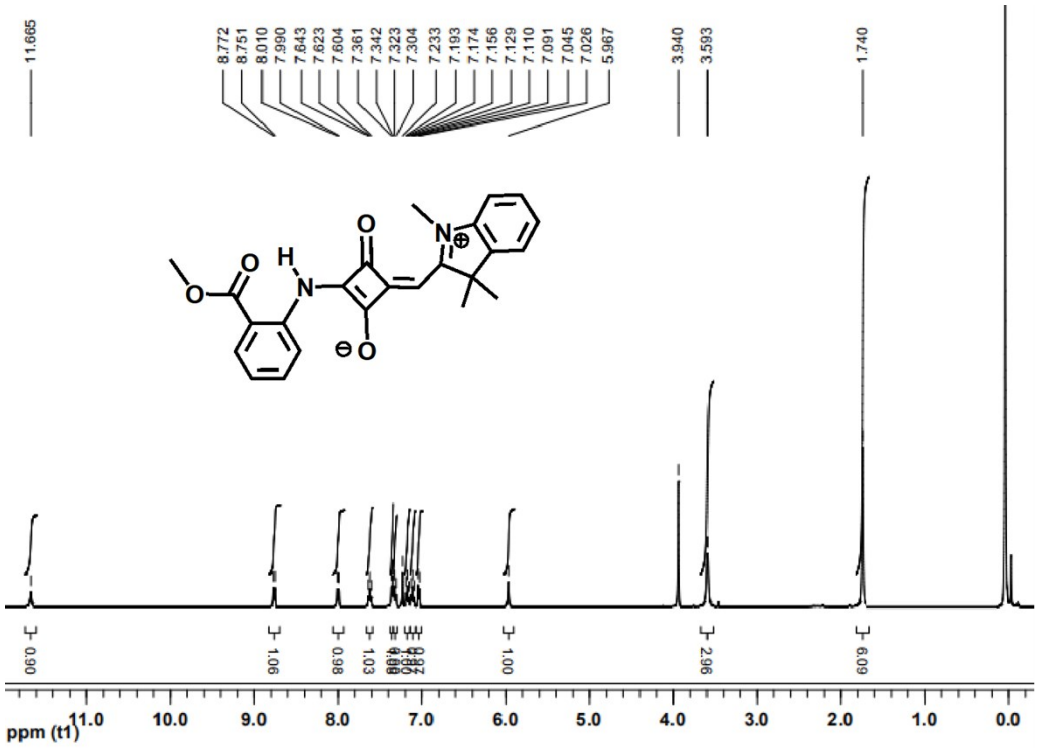

Figure S16. ^{1}H NMR spectrum of target **SQP** in $CDCl_3$.

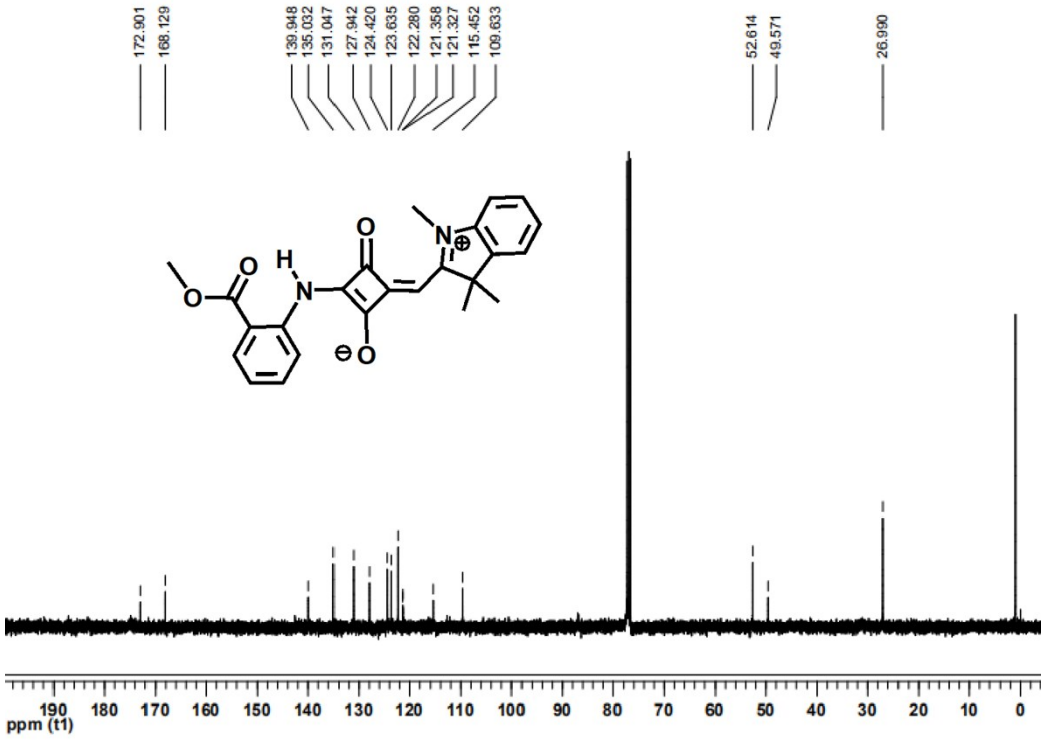

Figure S17. ^{13}C NMR spectrum of target **SQP** in $CDCl_3$.

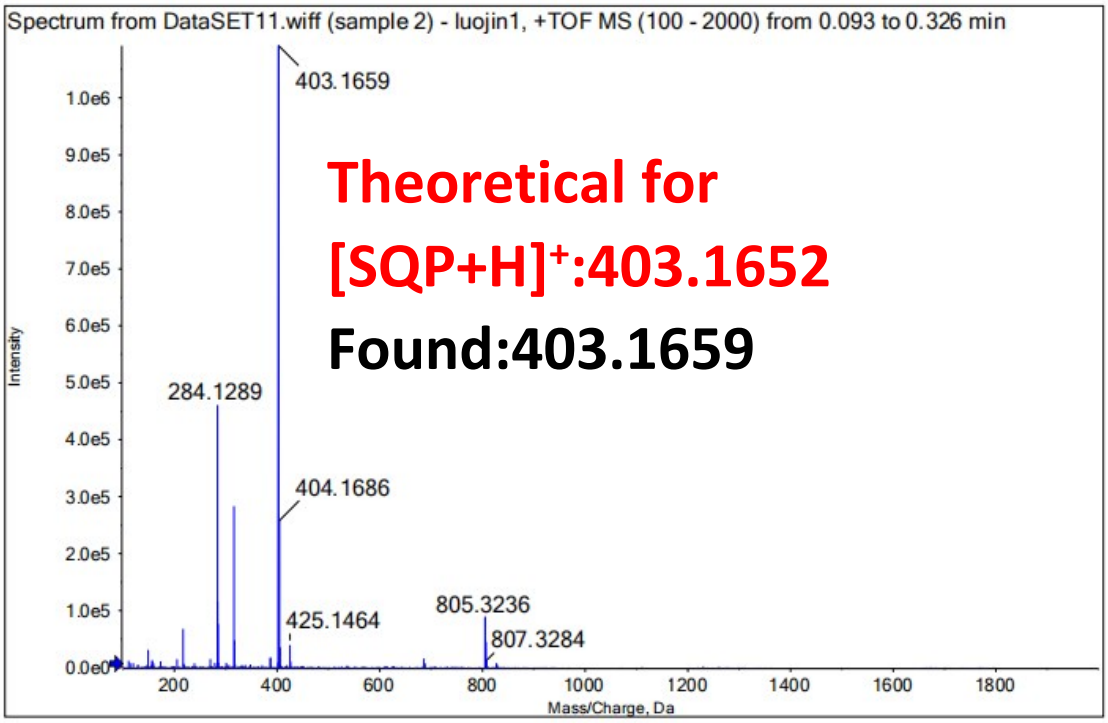

Figure S18. Mass spectrum of target **SQP**.

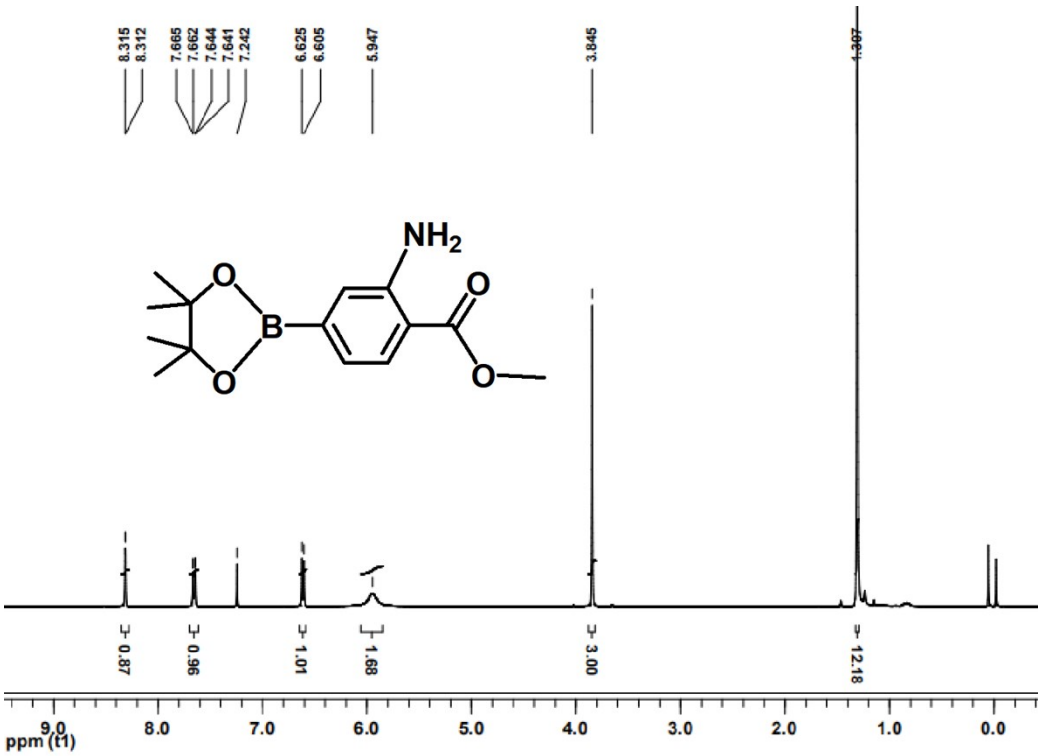

Figure S19. ^{1}H NMR spectrum of phenylboronic acid pinacol ester **a** in $CDCl_3$.

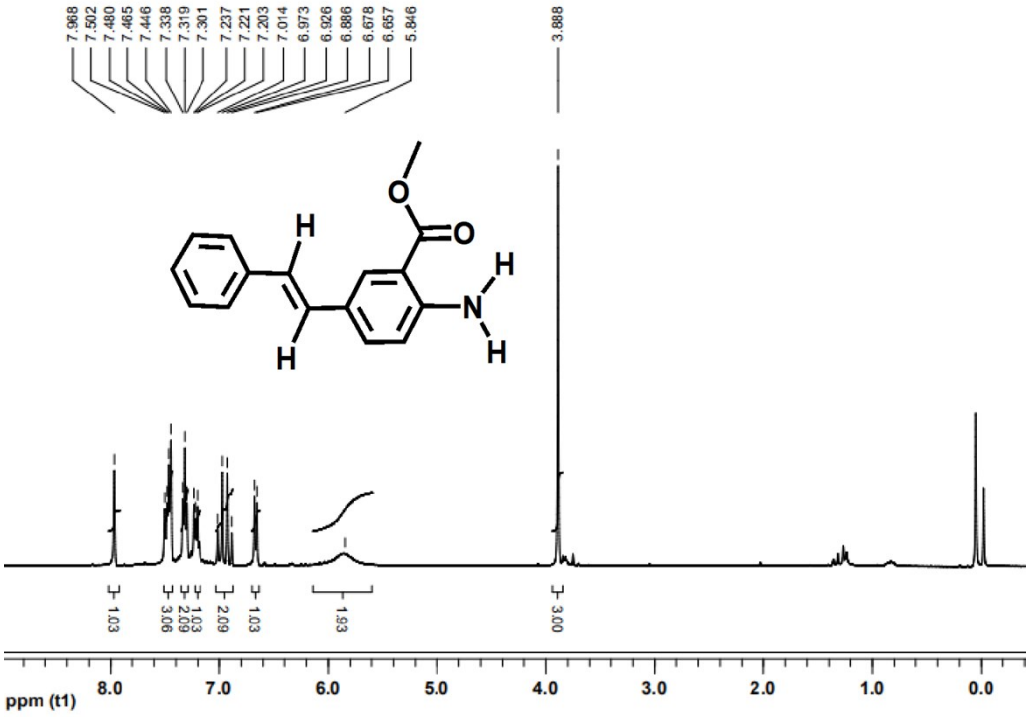

Figure S20. ^{1}H NMR spectrum of target **DPa** in $CDCl_3$.

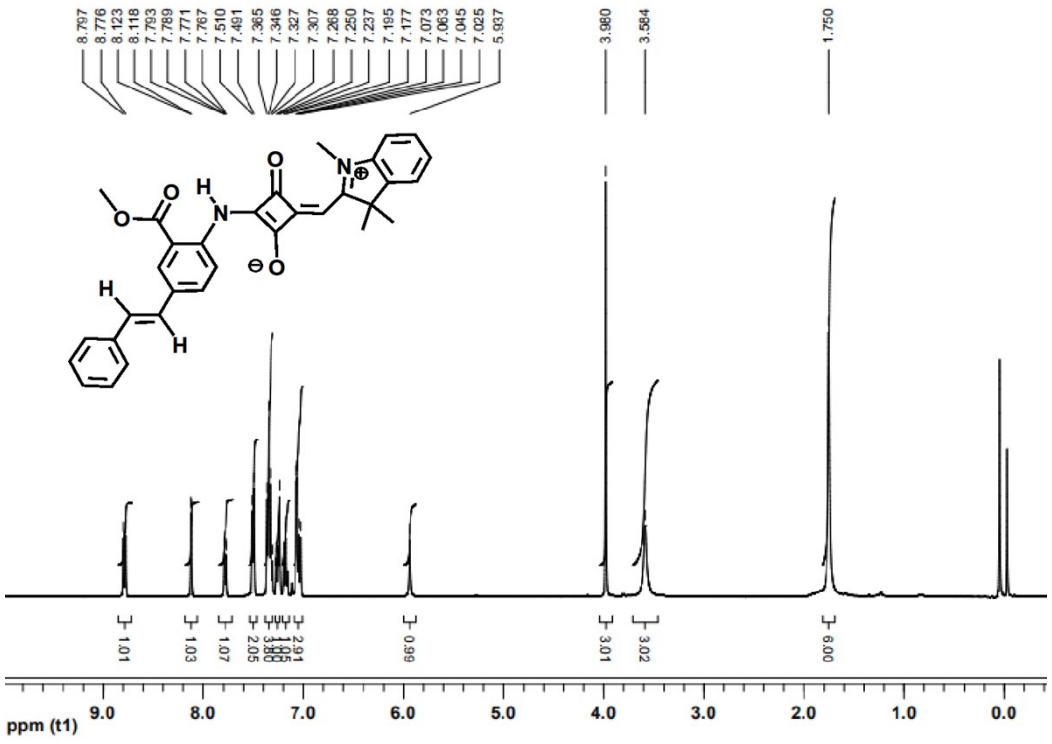

Figure S21. ^{1}H NMR spectrum of target **SQDP** in $CDCl_3$.

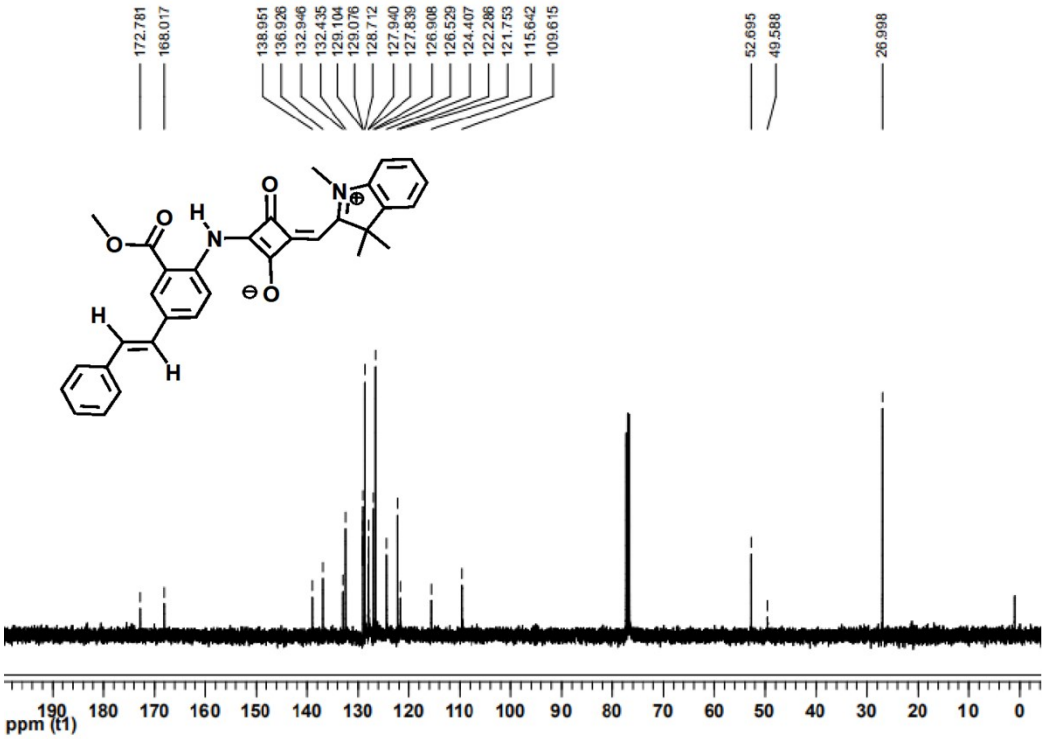

Figure S22. ^{13}C NMR spectrum of target **SQDP** in $CDCl_3$.

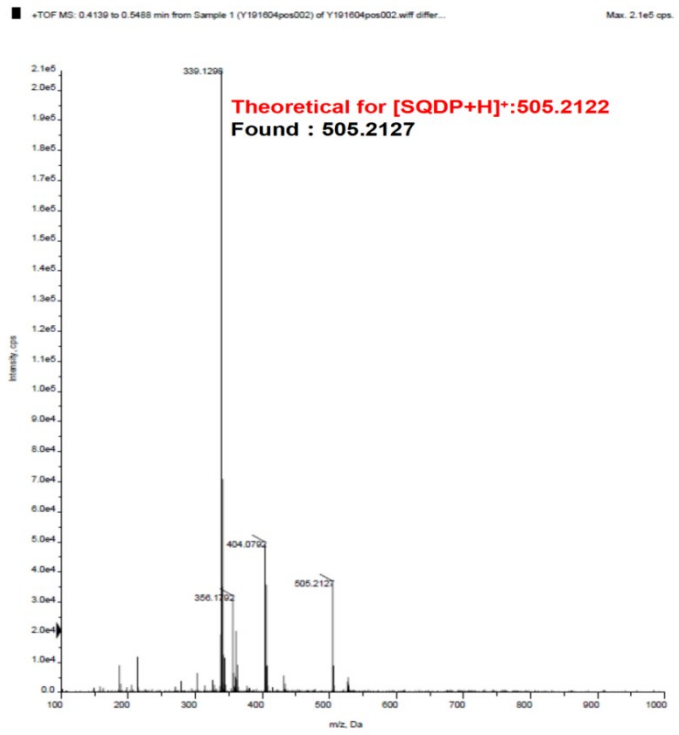

Figure S23. Mass spectrum of target **SQDP**.

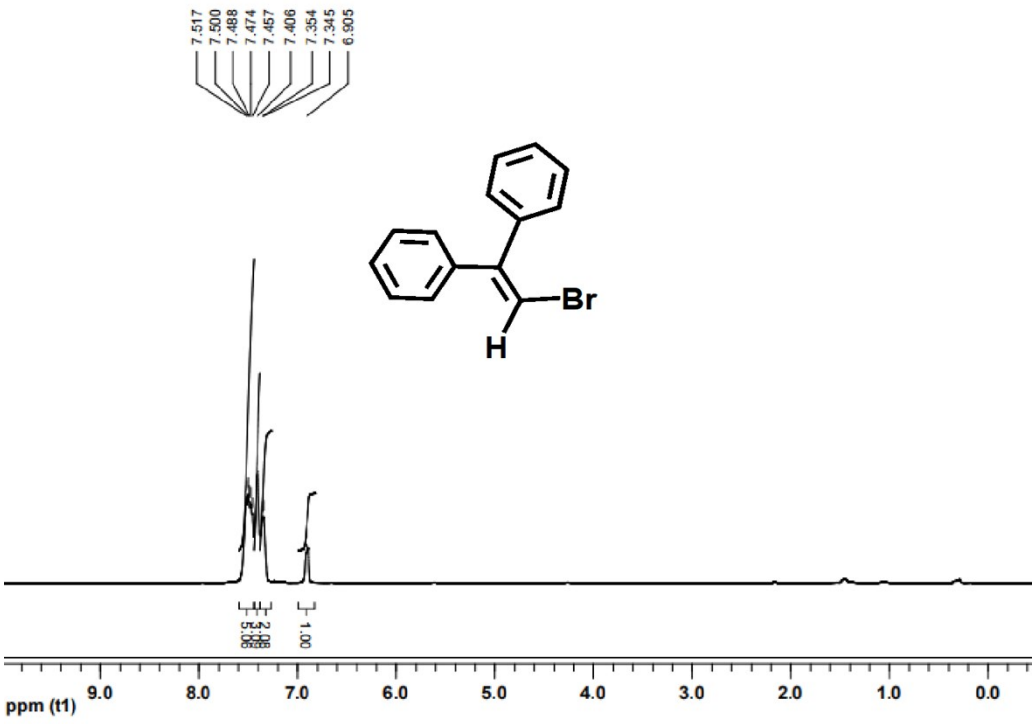

Figure 24. ^{1}H NMR spectrum of target **BrHTPE** in $CDCl_3$.

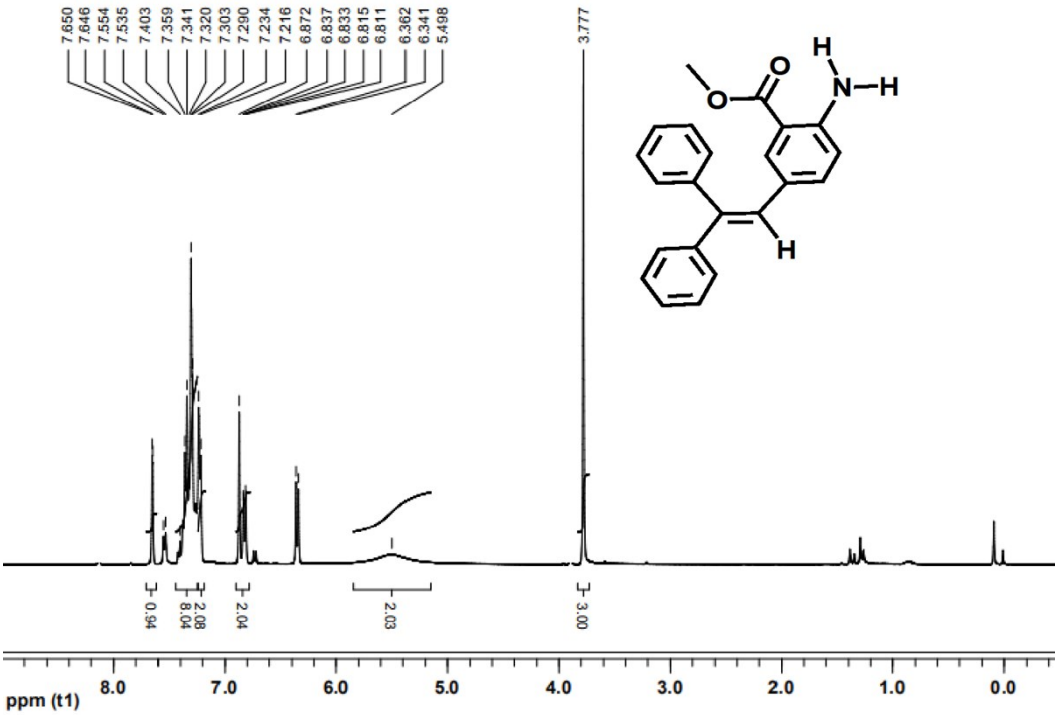

Figure 25. ^{1}H NMR spectrum of target **HTPEa** in $CDCl_3$.

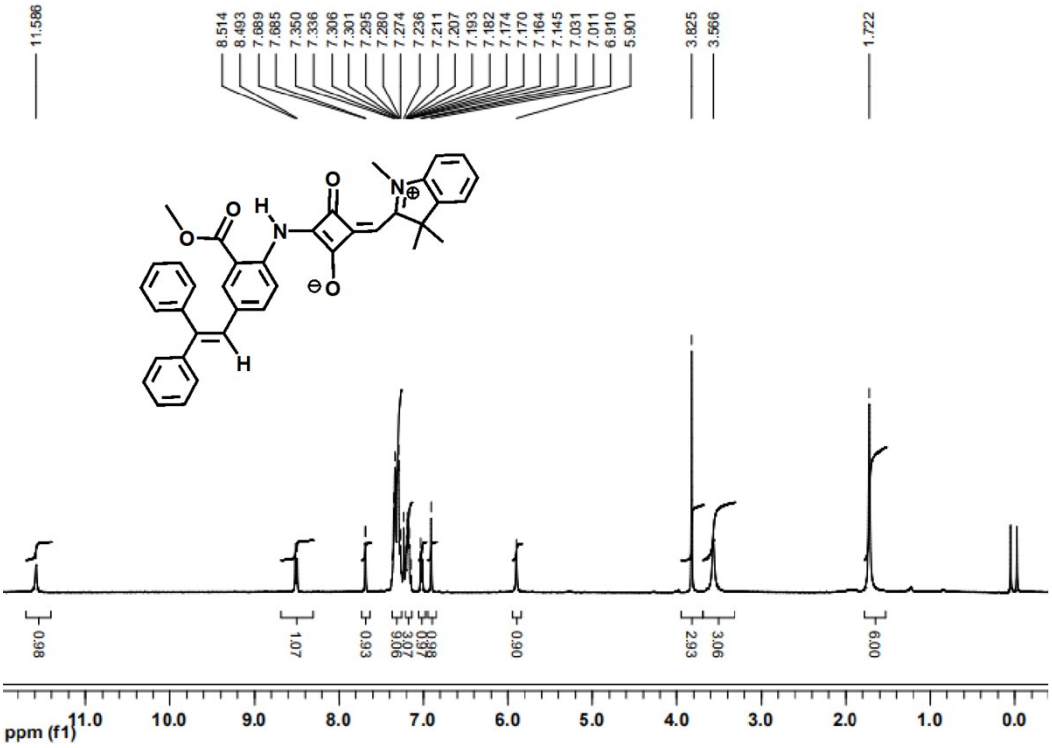

Figure 26. ^{1}H NMR spectrum of target **SQHTPE** in $CDCl_3$.

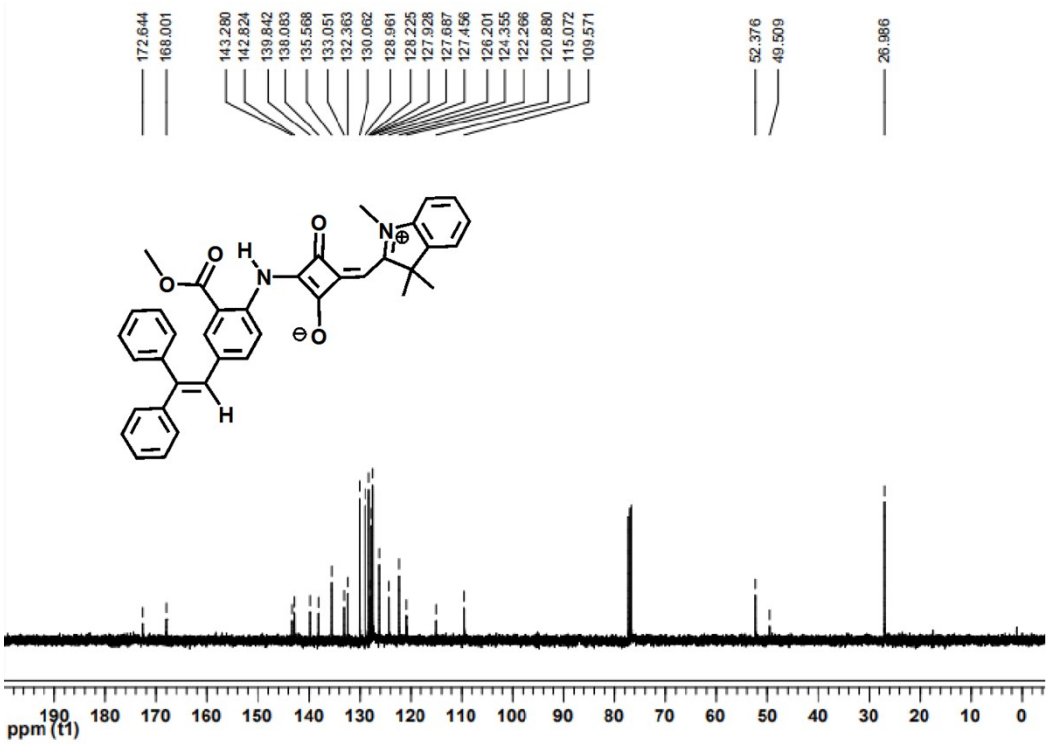

Figure 27. ^{13}C NMR spectrum of target **SQHTPE** in $CDCl_3$.

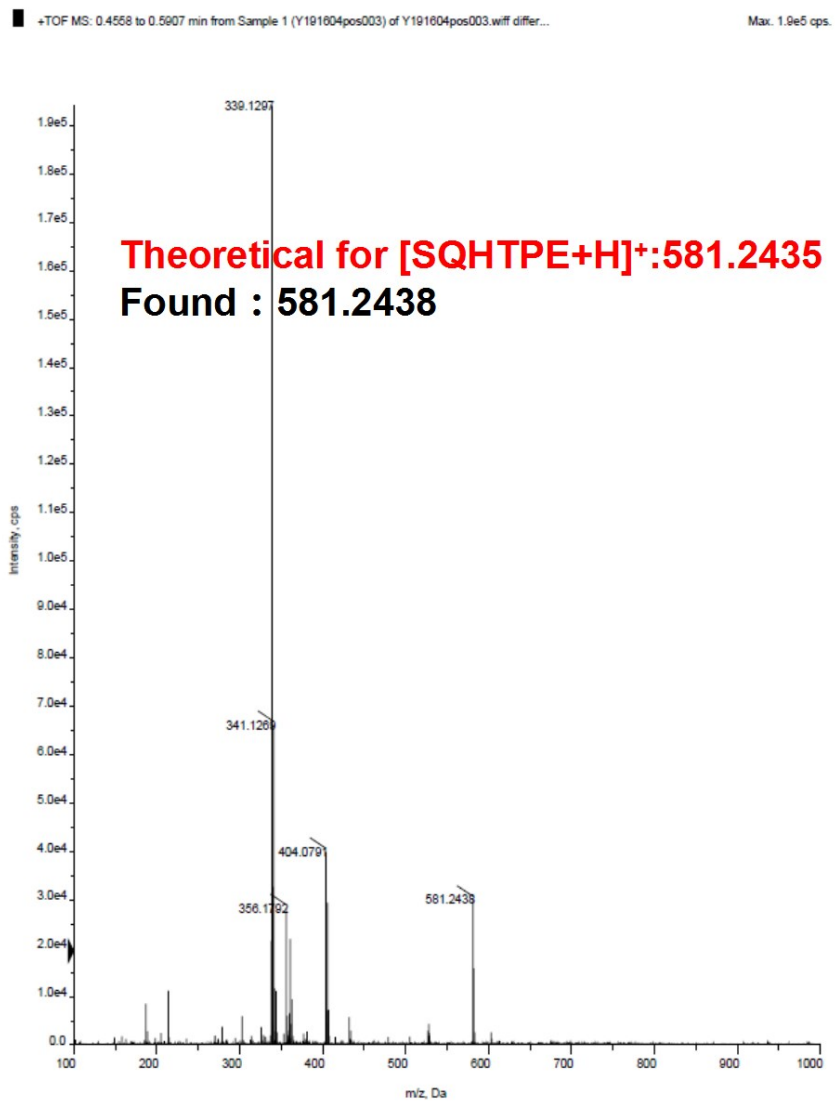

Figure 28. Mass spectrum of target **SQHTPE**.

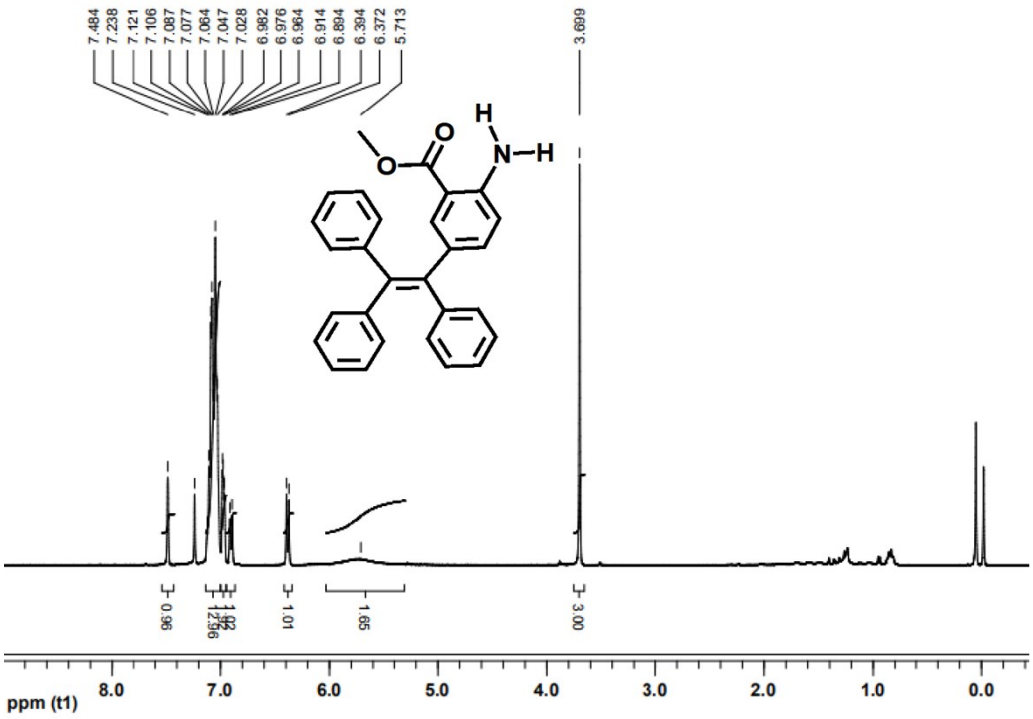

Figure 29. ^{1}H NMR spectrum of target **TPEa** in $CDCl_3$.

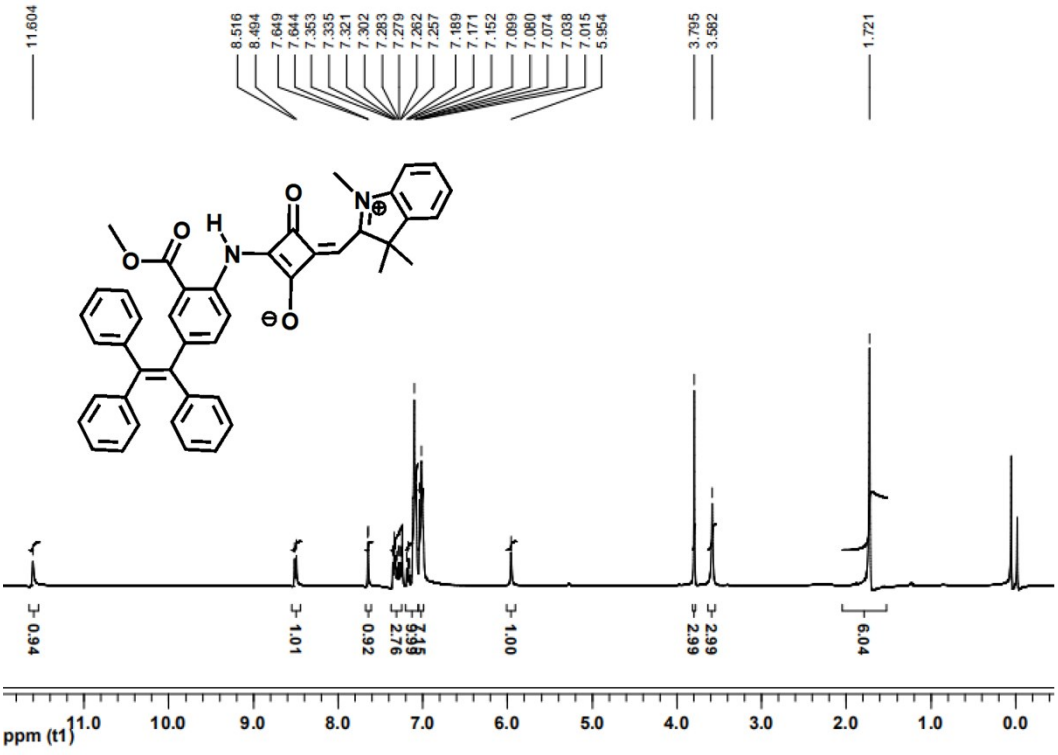

Figure S30. ^{1}H NMR spectrum of target **SQTPE** in $CDCl_3$.

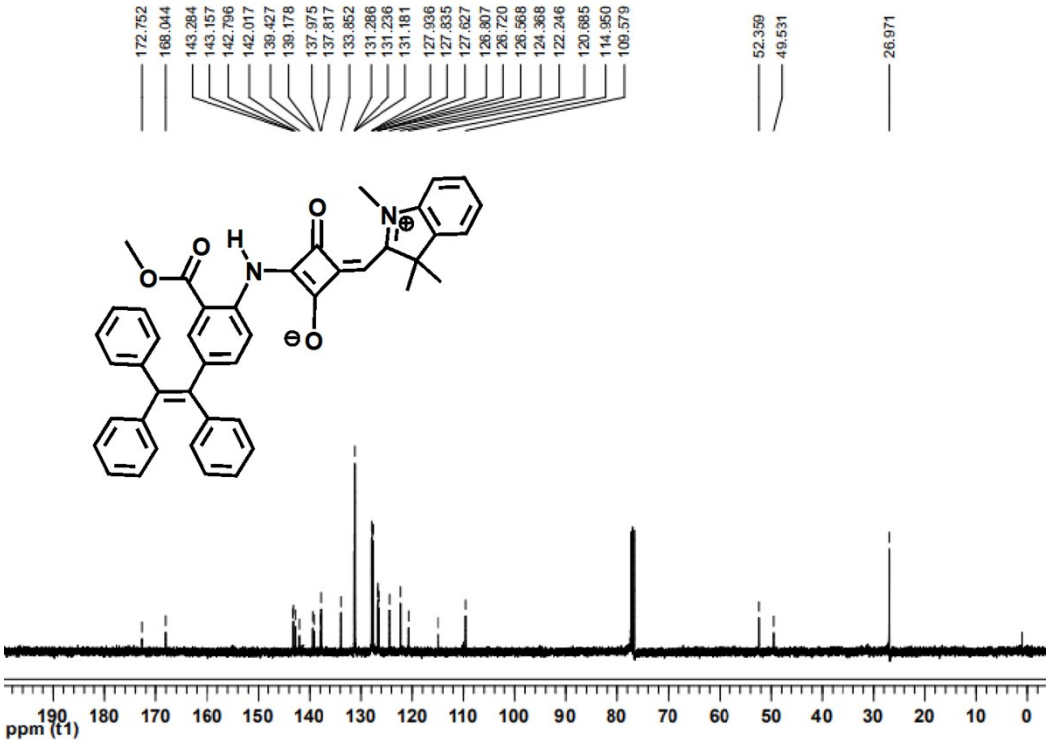

Figure S31. ^{13}C NMR spectrum of target **SQTPE** in $CDCl_3$.

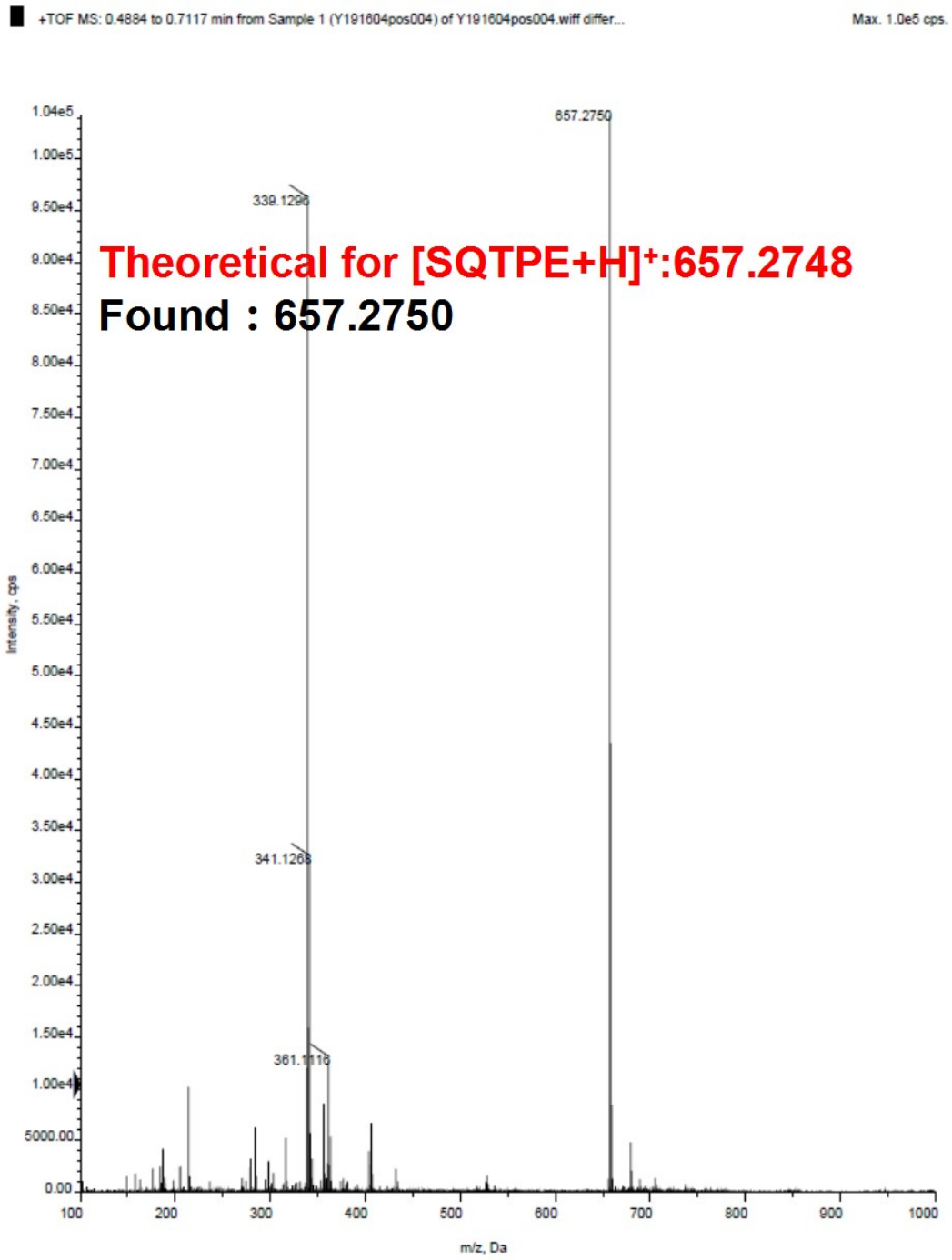

Figure S32. Mass spectrum of target **SQTPE.**

8 Reference

[1] M. J.Frisch, G. W. Trucks, H. B. Schlegel, G. E. Scuseria, M. A. Robb, J. R. Cheeseman, G. Scalmani, V. Barone, B. Mennucci, G. A. Petersson, H. Nakatsuji, M. Caricato, X. Li, H. P. Hratchian, A. F. Izmaylov, J. Bloino, G. Zheng, J. L. Sonnenberg, M. Hada, M. Ehara, K. Toyota, R. Fukuda, J. Hasegawa, M. Ishida, T. Nakajima, Y. Honda, O. Kitao, H. Nakai, T. Vreven, J. A. Jr. Montgomery, J. E. Peralta, F Ogliaro, M. Bearpark, J. J. Heyd, E. Brothers, K. N. Kudin, V. N. Staroverov, R. Kobayashi, J. Normand, K. Raghavachari, A. Rendell, J. C. Burant, S. S. Iyengar, J. Tomasi, M. Cossi, N. Rega, J. M. Millam, M. Klene, J. E. Knox, J. B. Cross, V. Bakken, C. Adamo, J. Jaramillo, R. Gomperts, R. E. Stratmann, O. Yazyev, A. J. Austin, R. Cammi, C. Pomelli, J. W. Ochterski, R. L. Martin, K. Morokuma, V. G. Zakrzewski, G. A. Voth, P. Salvador, J. J. Dannenberg, S. Dapprich, A. D. Daniels, O. Farkas, J. B. Foresman, J. V. Ortiz, J. Cioslowski, and D. J. Fox, Gaussian, Inc., Wallingford CT, **2009**.

[2] C. T. Lee, W. T. Yang, R. G. Parr, *Phys. Rev. B* **1988**, 37, 785.

[3] A. D. Becke, *J. Chem. Phys*. **1993**, *98*, 5648-5652.

[4] M. H. Sleiman, S. Ladame, *Chem. Commun.* **2014**, 50, 5288-5290.

[5] T. Luo, C. Liu, S. V. Eliseeva, P. F. Muldoon, S. Petoud, N. L. Rosi, *J. Am. Chem. Soc.* **2017**, 139, 9333-9340.

[6] G. Zhang, R. Bai, C. Li, C. Feng, G. Lin, *Tetrahedron* **2019**, *75*, 1658-1662.

[7] I. Ino, L. Wu, M. Munakata, T. Kuroda-Sowa, M. Maekawa, Y. Suenaga, R. Sakai, *Inorg. Chem.* **2000**, 39, 5430-5436.